Bio-inspired swimming and flying – Vortex dynamics and fluid/structure interaction

Ramiro Godoy-Diana

Bio-inspired swimming and flying

Vortex dynamics and fluid/structure interaction

Ramiro Godoy-Diana

Chargé de recherches au CNRS

Document presented to obtain the *Habilitation à Diriger des Recherches*
Université Pierre et Marie Curie

Jury presiding the HDR defense on December 16, 2014:

Frédéric Boyer (École de Mines de Nantes, Rapporteur)
Jérôme Casas (Université de Tours)
Matthias Heil (University of Manchester)
Maurice Rossi (Université Pierre et Marie Curie, Président du Jury)
Lionel Schouveiler (Université Aix-Marseille, Rapporteur)
Geoffrey Spedding (University of Southern California, Rapporteur)

Abstract

The present document, prepared in view of obtaining the *Habilitation à diriger des recherches*, reviews my main research subject at PMMH since 2006, which concerns the study of swimming and flying inspired by nature. Canonical examples of flapping flight and undulatory swimming are explored using simplified experimental models as a starting point. This allows for the discussion of some fundamental questions related to the physics of bio-inspired locomotion at "intermediate" Reynolds numbers. In particular, we address the strong fluid-structure interactions that arise in these problems, where we have focused on: simplified models of flapping foils in hydrodynamic tunnel experiments, especially in the dynamics of vorticity in the wake of an oscillating foil ; mechanical models of flapping flyers with flexible wings in a self-propelled configuration (in the spirit of the pioneer experiments of Etienne-Jules Marey), as well as novel experimental models of undulatory swimming.

Ramiro Godoy-Diana
Paris, 2014

Physique et Mécanique des Milieux Hétérogènes (PMMH)
UMR 7636 CNRS, ESPCI ParisTech, UPMC (Paris 6), UPD (Paris 7)
10 rue Vauquelin, 75005 Paris, France

"I’m as much in the dark as ever, though I’ve grown used in a sense to my obtuseness."

Henry James
The figure in the carpet

Avant-propos

Je présente ici une synthèse des travaux que j'ai développés au PMMH depuis 2006 sur la thématique de la propulsion "bioinspirée". J'ai divisé ce mémoire en 4 chapitres principaux plus une introduction et un point de perspectives à la fin. Le tout sauf cet avant-propos est écrit en anglais, histoire de pouvoir partager ceci avec plus de monde... Les travaux décrits dans ces pages sont pour la plupart le fruit d'un travail en équipe. Je tente ici une brève histoire, mentionnant les collaborateurs principaux de ces dernières années. Par ordre plus ou moins chronologique et avec un grand merci à tout le monde.

Depuis mon recrutement au PMMH en 2006, mon objectif a été de développer une activité autour des problèmes de mécanique des fluides liés à la propulsion animale à "grand" nombre de Reynolds (les guillemets pour dire que grand peut être de l'ordre de 100 dans certains cas, ce qui ferait rire à un aérodynamicien). À l'époque la thématique était nouvelle pour moi et j'ai pu compter sur l'enthousiasme et bon conseil de José Eduardo Wesfreid, qui m'a encouragé à proposer ce sujet pour mon projet au CNRS (¡Gracias Jefe!). Je me suis donc naturellement intégré à l'équipe Instabilités, Contrôle et Turbulence, où j'ai pu aussi collaborer avec d'autres gens, en particulier avec Jean-Luc Aider qui venait d'arriver au laboratoire avec plusieurs projets autour du contrôle. Le début de la période qui concerne ce rapport corresponde aussi à l'arrivée de Catherine Marais [1], d'abord en stage de M2 et après doctorante, co-encadrée par J. E. Wesfreid et moi-même.

En 2008, après une recherche de collaborateurs potentiels dans le paysage français et européen, nous avons mis en place un partenariat avec Jérôme Casas de l'Institut de recherches sur la biologie de l'insecte (IRBI) à l'Université de Tours et Laurent Jacquin du Département d'Aérodynamique Fondamentale de l'ONERA pour écrire un projet dédié à la "Physique des ailes battantes inspirées de l'insecte". Le projet, que j'ai coordonné, à reçu un financement de l'ANR dans le cadre du programme Blanc et nous a donné les moyens de faire mûrir petit à petit cette thématique. Le projet a été mené à terme avec succès, en changeant en cours de route plusieurs des objectifs initiaux, surtout pour suivre des nouvelles idées chez tous les partenaires.

En ce qui concerne le travail au PMMH le point crucial a été de diriger notre attention aux problèmes d'interaction fluide-structure liés non seulement à la propulsion par ailes battantes mais aussi ouvrant la porte à l'étude d'autres systèmes de propulsion bio-inspirés comme par exemple la nage ondulatoire. Cette redéfinition des priorités a été le fruit d'une collaboration fondamentale de ces dernières années, celle avec Benjamin Thiria, Maître de conférences à l'Université Paris Diderot, qui est arrivé au PMMH en 2009 et avec qui nous avons peu à peu établi une petite équipe "Nage et Vol bio-inspirés" en dirigeant ensemble les projets de plusieurs étudiants. Nous avons encadrés notamment Sophie Ramananarivo (doctorante 2010-2014) [2] et Verónica Raspa (post-doc 2010-2013), dont les travaux constituent une partie importante des résultats commentés dans ce mémoire. Les thématiques se diversifient en ce moment, d'une part en ce qui concerne la locomotion bio-inspirée, en considérant des problèmes de dynamique collective (thèse de Intesaaf Ashraf, 2014-2017), de miniaturisation des nageurs (thématique menée par Miguel Piñeirua, post-doctorant 2014-2015 dans le groupe) ou des régimes transitoires (thèse de Marion Segall sur la manoeuvre d'attaque des serpents en collaboration avec

l'équipe d'Anthony Herrel au MNHN, 2015-2017); et d'autre part explorant d'autres applications de l'interaction fluide-structure tels que la conversion d'énergie par des structures souples. J'en parlerai un peu dans la partie perspectives.

J'ai décidé de ne recueillir dans ce mémoire d'HDR que les travaux concernant la propulsion, en excluant ainsi une partie de mon activité de recherche de ces dernières années, qui concerne surtout ma collaboration avec José Eduardo Wesfreid sur les instabilités de sillage. Notamment, pour une partie de la thèse de Catherine Marais nous avons collaboré avec Dwight Barkley sur la réponse impulsionnelle du sillage d'un cylindre en régime sous-critique [3]. Puis, dans le cadre du Laboratoire Internationale Associé "Physique et Mécanique des Fluides" (France-Argentine), nous collaborons avec Juan D'Adamo sur les instabilités des sillages forcés [4; 5]. J'ai aussi gardé un oeil ouvert sur mes travaux précédant mon arrivée en France sur l'énergie de la houle [6], thématique qui restera d'actualité avec la perspective de nouveaux projets autour des énergies renouvelables.

Parmi d'autres collaborateurs que je n'ai pas cité ci-dessus, je voudrais notamment mentionner D. Pradal (Mécanicien au PMMH qui a conçu et fabriqué plusieurs des montages expérimentaux dont on parlera dans la suite) ainsi que toute l'équipe de l'atelier du PMMH qui a un moment ou un autre ont participé au montage des manips. Aussi un grand merci à G. Bimbard (doctorante à l'IRBI), D. Kolomenskiy (Postdoctorant a l'U. de McGill), O. Marquet (Chercheur à l'ONERA-DAFE), R. Fernández-Prats et F. Huera-Huarte (Universitat Rovira i Virgili), G. Spedding (USC) et R. Zenit (UNAM) qui ont été des interlocuteurs importants à différents moments de ces dernières années.

Un mot sur les finances : en complément des ressources fournis par les organismes de tutelle du laboratoire PMMH (ESPCI, CNRS, UPMC et U Paris Diderot), les travaux décrits dans ce document ont été financés par l'Agence Nationale de la recherche (Project ANR-08-BLAN-0099, *The physics of insect-inspired flapping wings*, 2008-2012, PI : R. Godoy-Diana) et la Fondation EADS (Projet *Fluids and elasticity for biomimetic propulsion*, 2012-2014, PI : R. Godoy-Diana & B. Thiria). Pour avoir fait tourner toute cette machinerie, un chaleureux remerciement à l'équipe administratif du PMMH, Fred et Claudette aujourd'hui, Amina, Claudine,... hier. Ainsi qu'aux directeurs Philippe et Eduardo.

Et il ne me reste qu'un petit bout de page pour dire merci à nouveau ! Merci aux membres du jury qui vont lire les pages qui suivent, double merci aux rapporteurs qui devront écrire en retour. Merci à tous mes profs, étudiants, collègues et amis qui, au PMMH et ailleurs, ont partagé coeur et cerveau en sachant (ou peut être pas) que le retour sur investissement serait maigre. Un abrazo fuerte también a la familia, en especial a Sebas y Malena que me toleran en casa al grito de "¡Papá, ya no trabajes el fin de semana!"...

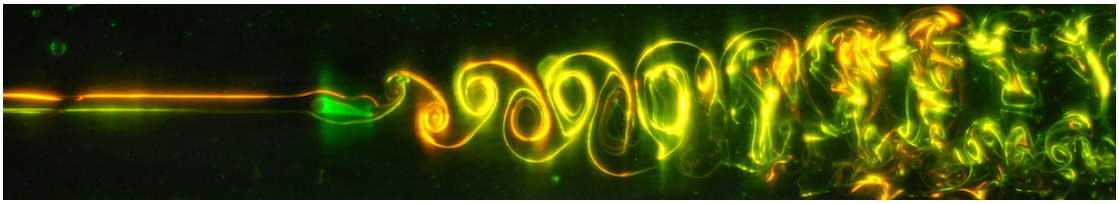

Contents

1. Introduction

The following pages deal with various problems related to swimming and flying in nature. Aside from their evident biological relevance, the locomotion strategies found in nature in the flight of birds, bats and insects and the swimming of fish and marine mammals have long since served as inspiration for the development of artificial systems. The result of this pluridisciplinary appeal is that literature abounds over an ample spectrum of approaches bounded by biology, physics and engineering. Not pretending to give an exhaustive review of these vast domains, we will start by pointing out here a few key issues, as well as some of the works that have been important in guiding our attempt to develop simplified models of flapping flyers and undulatory swimmers. Along the way we will hint on the questions that we have asked and, additionally, recall some of the customary analytical tools that have been proven useful in the quest for reasonable answers.

1.1 Flying

We will focus here in problems related to powered flapping flight, excluding thus some fascinating problems of aerial locomotion found in nature such as gliding or parachuting. From the biological point of view, the latter have not only been probable precursors of powered flight, but besides they constitute an ecologically advantageous strategy on their own. And it is needless to say that they have also inspired human-made devices —quoting Buzz Lightyear: *"This is not flying, this is falling with style!"*. From the engineering perspective, gliding can be described using fixed-wing aerodynamics, something that does not work for flapping wings. In a conventional aerodynamic picture, the basic model considers an airfoil immersed in an externally imposed flow, which results in the production of lift and drag forces. Lift opposes the weight of the flying thing, while drag opposes thrust (see Fig. 1.1). The latter is thus provided independently of the wing, using a propeller, and determines the fundamental difference with flapping-powered flight,

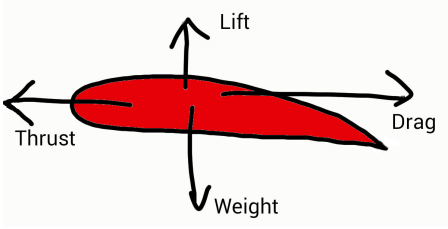

Figure 1.1: Schematic diagram of forces on a wing section.

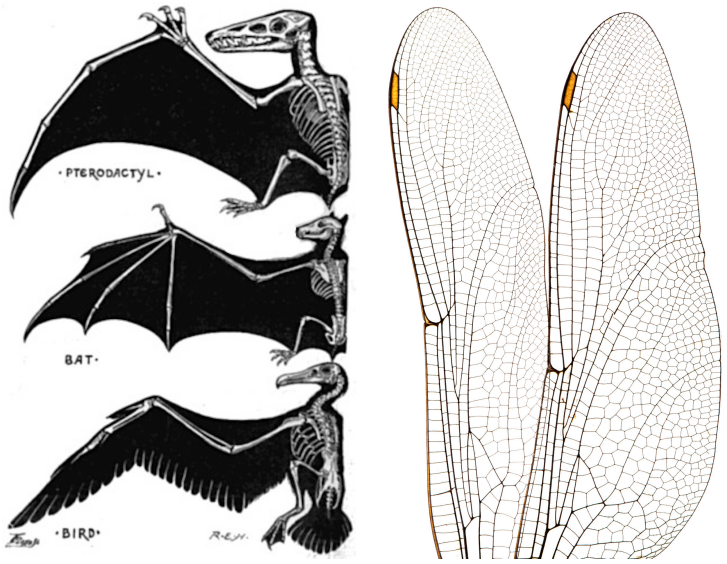

Figure 1.2: Left: Wing of Reptile, Mammal, and Bird (From G. J. Romanes, 1892 [11]). Right: Dragonfly wings (Photo credit: P. Kratochvil).

where both lift and thrust are produced by the moving wing. This results in the appearance of a collection of unsteady mechanisms that are crucial components of the aerodynamic force balance [see e.g. 7; 8]. As we will comment in more detail below, the dynamics of vortices around the wings plays a fundamental role concerning the mechanisms of unsteady force production.

Coming back to the realm of the living, four animal groups have evolved powered flight independently [9]. In addition to fuelling our intimate awe toward nature, this observation points our reflection to the concept defined by biologists as *evolutionary convergence* [10]: The fact that evolution has independently given rise in different non-related species to analogous structures that share form and function, as a result of their adaptation to similar environments. The reason for convergent evolution is the simple fact that a given trait gives a strong advantage to a species once it has appeared. And flight is definitely a particularly successful strategy for many reasons that range from local flight, such as escaping predators, catching prey or finding resources, to migration, where a whole population can move from one place to another, for instance following more favourable weather [9].

The wings of birds, bats and the now extinct pterosaur are all versions of a modified forelimb (see Fig. 1.2). In the case of insects on the contrary, wings come from a different body part altogether, as an independent structure attached to the upper part of the thorax, while the legs are attached to the bottom. Insects were also the first group to evolve powered flight, and they are the only winged invertebrates.

Insects cannot control the shape and motion of the wings within the wing itself as vertebrates do, since they do not have joints or muscles out in the wing. They have however a branching arrangement of veins that carry blood and air passages that can be used to control the stiffness of the wing [12]. These veins in certain insects work as springs and hinges permitting the wing

structure to fold. Insect wings are thus compliant structures [13] and their elastic properties are certainly a fundamental issue of the mechanics of their flapping-based aerodynamic force production [14]. Part of the works reviewed here have been devoted to the study of such a fluid-elasticity problem, where the observation of insect wings in motion have served as inspiration for the development of laboratory models.

1.2 Swimming

We will not converse a lot here about the diverse diving and splashing feats achieved by humans, but a little about more professional swimmers such as fish. Using body undulations to produce a propulsive force is a widespread technique embraced by many different organisms over a wide range of scales [15]. Physically, as we will discuss further below, the size of the organism determines the type of forces at play in the dynamical balance of the locomotion problem: microscopic swimmers such as sperm or flagellated bacteria evolve in a dynamical environment entirely governed by viscous friction [see e.g. 16], whereas in macroscopic organisms like aquatic vertebrates, friction forces are confined to a thin region surrounding the body —the boundary layer— and the production of a propulsive force relies also upon inertial momentum transfer to the fluid [see e.g. 17]. However, some features appear as crucial for every swimmer regardless of its size, such as the establishment of a propagative kinematics for the undulating wave that describes the body deformations. This question is at the core of the fluid-structure interaction problem of the artificial swimmers that appear in the following pages.

In what follows we will focus mostly on these *inertial* fish-like swimmers. The locomotion of fish or, more generally, of aquatic vertebrates has been extensively studied, in the first place from the biological perspective [18; 19], but also as a source of inspiration for engineering applications [20; 21]. Different strategies to produce locomotive forces for swimming are found in nature (see Figure 1.3), which can be broadly separated in median and paired fin propulsion (MPF) and body and caudal fin propulsion (BCF) [19; 22; 23]. On the latter category one can further distinguish the periodic steady regime observed during cruising, from transient manoeuvres such as sharp turns and fast starts. It has been shown that the main locomotor strategy observed in a given species is linked to the feeding problem: for instance, BCF steady swimmers feed from a widely dispersed source whereas species constantly performing transient fast-start and turn maneuvers rely on locally-abundant prey such as fish schools [22].

Aquatic vertebrates rely on muscular action distributed all along the body to prescribe the kinematics of any given swimming gait. And it has been shown that the wave of muscle activation travels down the fish much more rapidly than the wave of bending [24]. Speaking of bio-inspiration or biomimetism, the design elements of an artificial swimmer or flyer that one would like to copy from an animal can be envisaged at different levels. One approach is to reproduce a solution found in a real animal, say, an anguilliform swimmer, using sophisticated actuation and control to fine-tune a given body kinematics that has been "tested and approved" by nature to perform efficiently for a given task [1]. Impressive examples of this can be found in the literature, such as the robotic eel of EPFL's Biorobotics Lab [25] or MIT's robotuna [26].

1. I had written here "...to be optimal for a given task" but I am evading the debate on optimality in the multi-dimensional space of evolution...

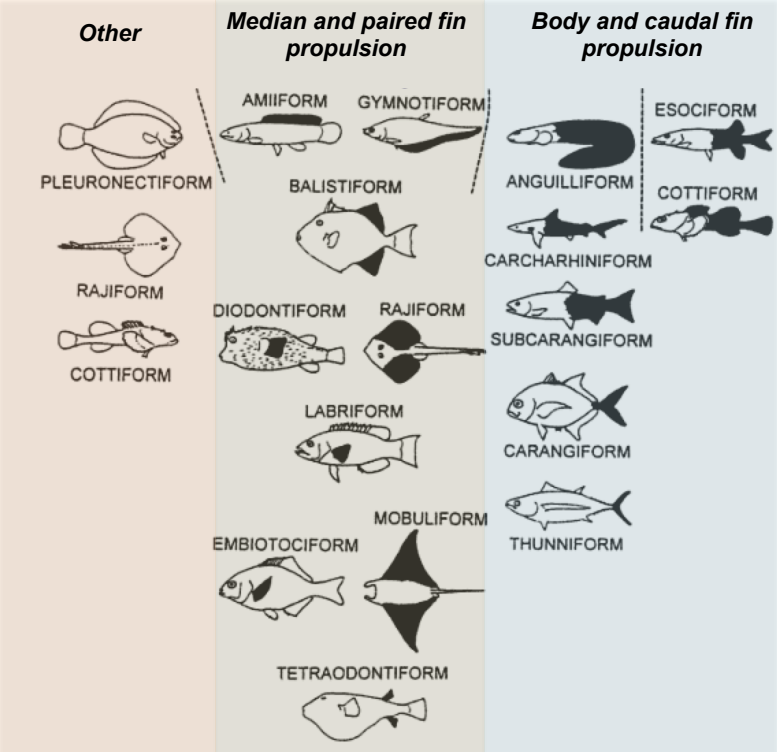

Figure 1.3: Swimming modes (modified from Webb, 1994 [23]).

In our work on bio-inspired swimmers a different approach has been pursued, one where the kinematics is not actively enforced, but is the passive outcome of the body elasticity of model swimmers where the actuation is localised: a strong fluid-structure interaction problem that has received considerable attention recently [see e.g. 27–29].

1.3 Fluid-structure interaction

In these problems of *bio-inspired* propulsion, it is thus the active motion of a structure (e.g. a wing or a fin) that produces a propulsive force by its interaction with the surrounding fluid (e.g. air or water). From the fluid dynamics point of view, where the moving structure determines the boundary conditions for the fluid motion, the problem will be strongly dependent on the types of forces driving the dynamical balance in the *Navier-Stokes equations*

$$\frac{\partial \mathbf{u}}{\partial t} + (\mathbf{u}\cdot\nabla)\mathbf{u} = -\frac{1}{\rho}\nabla p + \nu\nabla^2\mathbf{u} + \frac{1}{\rho}\mathbf{F}\,, \tag{1.1}$$

$$\nabla\cdot\mathbf{u} = 0\,, \tag{1.2}$$

that describe the motion of the fluid. Eqs. 1.1 and 1.2 rule the dynamics of an incompressible

fluid of constant density ρ and constant kinematic viscosity ν, described by its velocity and pressure fields, $\mathbf{u}$ and p, respectively, and subject to an external force $\mathbf{F}$ (the derivation of these equations from basic principles can be found in any hydrodynamics textbook, e.g. [30]). Writing U and L for the characteristic velocity and length scales of the problem in question one can rewrite these equations as

$$\frac{\partial \mathbf{u}}{\partial t} + (\mathbf{u}\cdot\nabla)\mathbf{u} = -\nabla p + \frac{1}{\mathrm{Re}}\nabla^2\mathbf{u} + \mathbf{F}\,, \tag{1.3}$$

$$\nabla\cdot\mathbf{u} = 0\,, \tag{1.4}$$

where all variables are now dimensionless and $\mathrm{Re} = LU/\nu$ is the *Reynolds number*, which rules the aforementioned dynamical balance by settling the relative importance of inertial vs. viscous forces. The two limit cases in terms of Re have been widely studied: when $\mathrm{Re} \gg 1$ the viscous term is negligible and in practice the Euler equations for an ideal fluid are recovered, the pressure gradient being balanced by fluid inertia. In these high-Reynolds number flows, such as the flow around an airfoil, the effects of viscosity are confined to a thin *boundary layer* that matches over a small length scale the "outer" inviscid flow and the actual solid boundary, where the no-slip condition applies and the velocity of fluid particles must match the velocity of the boundary. In the other limit, for $\mathrm{Re} \ll 1$, it is the viscous term that governs the dynamics. This limit, known as Stokes flow, describes for instance the propulsion of microscopic organisms using cilia or flagella. The Reynolds numbers relevant to animal swimming and flying cover a broad range (see Table 1.1), a lot of cases being “intermediate” with respect to the two limits mentioned above, those that conventional analytical methods are capable of handling [31]. Physical insight relevant to this intermediate range usually requires the correct modelling of the vortex dynamics detaching from the swimmer or flyer and considerable efforts in this sense have been widely documented in the literature [see e.g. 32–34, and references therein]. Control of vortices produced by flapping wings or fins to generate propulsive forces is the everyday task of birds, insects and swimming animals. And many studies of actual flapping extremities have been indeed driven by the need for a better understanding of this form of propulsion with the ultimate goal of enhancing man-made propulsive devices [see extensive reviews in 21; 35–38].

Table 1.1: Cruising Reynolds numbers

Bacterium	$\sim 10^{-5}$
Marine invertebrate larvae	$\sim 0.1 - 10$
Drosophila	$\sim 10^{2}$
Small fish (e.g. guppy)	$\sim 10^{3}$
Dragonfly	$\sim 10^{4}$
Tuna	$\sim 10^{5}$
Blue whale	$\sim 10^{6}$

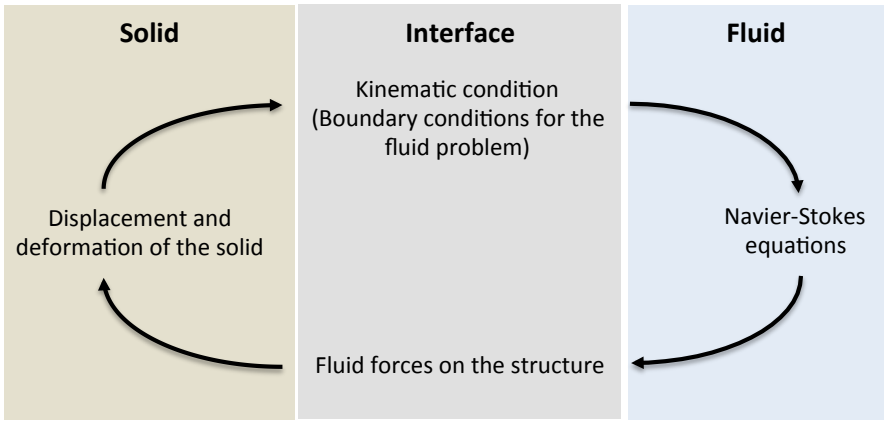

Reynolds number	Mass ratio	Elastoinertial number	Cauchy number	Elastoviscous number
$\mathrm{Re} \sim \frac{fluid\ inertia}{fluid\ viscosity}$	$\mathcal{M} \sim \frac{solid\ mass}{fluid\ mass}$	$\mathcal{N}_{ei} \sim \frac{solid\ inertia}{solid\ elasticity}$	$\mathcal{C}y \sim \frac{fluid\ inertia}{solid\ elasticity}$	$\mathcal{S}p \sim \frac{fluid\ viscosity}{solid\ elasticity}$

Figure 1.4: Schematic diagram of the fluid and solid dynamics two-way coupling in a fluid-structure interaction problem (inspired from Doaré, 2010 [39]) and some usual dimensionless numbers.

Now consider the motion of the structure, i.e. the swimmer or flyer. While it constitutes the boundary condition for the fluid problem, its own dynamics is of course coupled to that of the surrounding fluid, establishing the two-way coupling described schematically in Fig. 1.4. The dominant features of the different branches in this full fluid-structure interaction problem picture are ruled by various non-dimensional parameters that weigh the relative importance of the different physical mechanisms at play. Some of these numbers are built solely from the comparison of different dynamical properties of either the fluid (e.g. the Reynolds number) or the solid physics, but others are intrinsically built from the comparison between the dynamics of the fluid and the structure. The table in Fig. 1.4 summarises some of the dimensionless numbers that can be built considering a model system where a slender flexible structure of characteristic length scale L, thickness h and bending rigidity $B \sim Eh^3$ (e.g. a beam or a plate) propels itself through a fluid of density ρ and viscosity μ at an average cruising speed U as the result of a harmonic oscillation of angular frequency $\omega = 2\pi f$ and amplitude A_ω imposed at one of its ends. Such a simple model allows for the introduction of the key parameters that can be used to describe the locomotion problem of a flexible body in a fluid. We have already noted the dynamical regimes defined by the Reynolds number. Additionally, the mass ratio quantifies the effect of the surrounding fluid on the inertia term in the equation of motion of the structure, whereas $\mathcal{N}_{ei}$, $\mathcal{C}y$ and $\mathcal{S}p$ ponder, respectively, the solid inertia, the fluid loading (the dynamic pressure) and the viscous forces with respect to the elasticity of the structure.

In the following chapters we will develop further these ideas for two particular cases, a flapping wing in air and a slender undulatory swimmer in water. The fluid-structure coupling arises in different manners in these two cases, although the basic solid model can be described

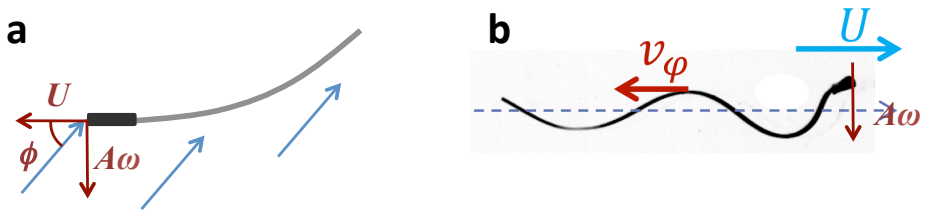

Figure 1.5: Beam model for a flapping wing (a) or an undulatory swimmer (b). The characteristic velocity of the imposed actuation $A\omega$ and the resulting cruising velocity U are represented schematically in both cases. Additionally indicated: for the flapping wing, the angle ϕ that characterises the ratio of these two velocities; and for the undulatory swimmer, the phase velocity of the bending wave v_φ.

by the same Euler-Bernoulli beam (see Fig. 1.5), described in the small amplitude regime by [see e.g 40]:

$$\mu h_{tt} + B h_{xxxx} + F_{NL} = \mathcal{F}_{f/s} + W(t)\ . \tag{1.5}$$

Here $h(x,t)$ is the lateral displacement of the beam (i.e. along a direction y perpendicular to the mean locomotion direction x), $\mathcal{F}_{f/s}$ is the effect of the fluid appearing as a force on the equation for the dynamics of the structure, and $W(t)$ is the imposed actuation, which for a flapping wing or fin can be usually modelled as above by a harmonic oscillation $\sim A_\omega \sin \omega t$.

But before considering the full fluid-structure interaction problem (that where the wing or fin is deformed under the action of the surrounding fluid), even the one-way problem where an effectively rigid but moving structure serves as boundary condition to the fluid problem can be non-trivial at these intermediate Reynolds numbers, in part because of the unsteadiness related to the dynamics of vorticity. We discuss in the following chapter some of the characteristic traits of the unsteady flows produced by a rigid structure oscillating in a fluid, focusing on a quasi-two-dimensional view of the vorticity dynamics in the wake of a very idealised flapping wing or fin.

1.4 Plan

This review is organised as follows: Chapter 2 is dedicated to our work using flapping foils in a hydrodynamic tunnel as a basic model to study vorticity dynamics in a simple propulsive wake. The chapter ends with a modified experimental setup with a self-propelled geometry where we explored the role of wake symmetry properties in the swimming performance. It is followed in Chapter 3 by the discussion of our flapping flyer models with flexible wings using a merry-go-round setup. Chapter 4 summarises our work with a real biological model, a Pierid butterfly, where we focused on a transient regime: the take-off maneuver. Our undulatory swimming studies are the subject of chapter 5 and, finally, the manuscript is closed in chapter 6 by a brief

account of current projects and perspectives. Chapters 2 to 5 open with a brief summary and a list of the corresponding references that are included in the selected publications appendix.

2. The flapping foil experiments

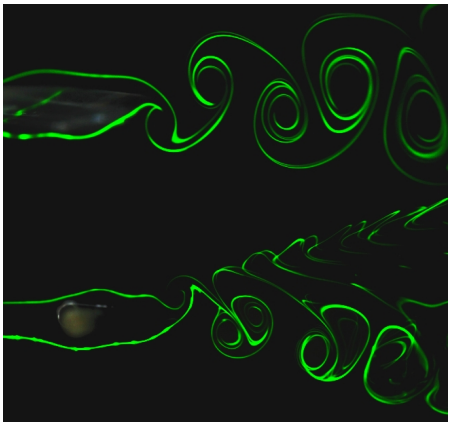

Figure 2.1: Fluorescein-dye visualisation of the vortex streets in the wake of a pitching foil. Flow is from left to right. On top the *reverse* Bénard-von Kármán wake, on bottom an asymmetric wake. (Figure from [41])

Summary

This chapter reviews our work on propulsive wakes using experiments with flapping foils. The goal of these studies was to explore simple models that contain key dynamical elements, such as the creation and organisation of vorticity, that are crucial in every system involving flapping wings or fins as a means of producing propulsive forces. The first part is devoted to the study of the wake of a rigid flapping foil, in particular to the establishment of an ubiquitous feature related to propulsive flapping motion, which is a vortex street with the sign of vorticity of each vortex reversed with respect to the typical Bénard-von Kármán (BvK) wake. We study the relationship between the evolution of the wake structure as a function of the flapping parameters and the drag-thrust transition [42], the symmetry breaking of the reverse BvK wake [41] and the effect of using a flexible foil instead of a rigid one [43]. We close this chapter opening a broader perspective on the problem of wake topology considering a two-foiled self-propelled swimmer [44].

Collaborators : C. Marais, V. Raspa, B. Thiria, J. L. Aider, J. E. Wesfreid

References :

Godoy-Diana, Aider, Wesfreid *Phys. Rev. E* **77**, 016308 (2008). [42]
Godoy-Diana, Marais, Aider, Wesfreid *J. Fluid Mech.* **622**, 23-32 (2009). [41]
Marais, Thiria, Wesfreid, Godoy-Diana *J. Fluid Mech.* **710**, 659-669 (2012). [43]
Raspa, Godoy-Diana, Thiria *J. Fluid Mech.* **729**, 377-387 (2013). [44]

2.1 Transitions in the wake of a flapping foil

The primary goal of our work on this subject was to use one of the simplest flapping models, a pitching foil, with careful measurements on a hydrodynamic tunnel setup to explore the basic features of one of the landmarks of these bio-inspired propulsive wakes: the *reverse* Bénard-von Kármán (BvK) vortex street (see Figures 2.1 and 2.2).

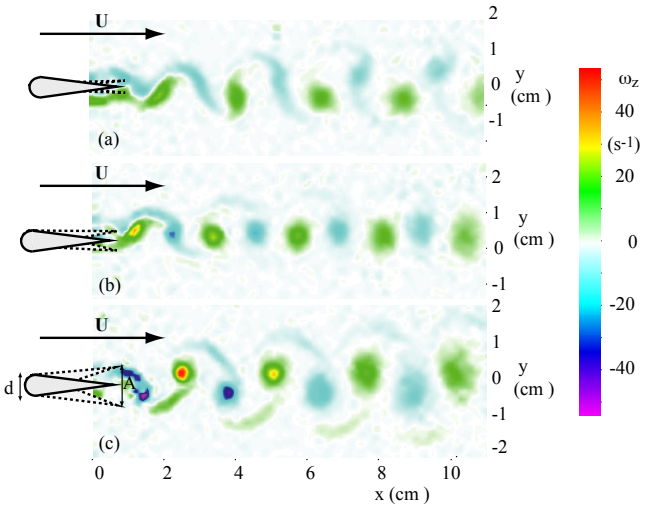

Figure 2.2: Transition from the Bénard-von Kármán wake (top frame) to a reverse wake (bottom frame) seen in the vorticity field behind a flapping foil obtained from PIV measurements in a hydrodynamic tunnel. The section of the foil is represented schematically. The Reynolds number based on the maximum width of the foil d was set to 255 (which corresponds to a chord-based Reynolds number of ~ 1200).

The indicator feature of this type of wake is a vortex street with the sign of vorticity of each vortex reversed with respect to the typical Bénard-von Kármán (BvK) vortex street behind a cylinder. Such reverse BvK vortex streets have not only been observed in the wakes of swimming fish [see e.g. 45; 46] but also studied in detail through laboratory experiments with flapping foils [47–54] and numerical simulations [50; 55–59]. In general, flapping-based propulsive systems, either natural or man-made, are often discussed in terms of the swept-amplitude-based Strouhal number [49; 60]:

$$St_A = fA/U_0 \,, \tag{2.1}$$

defined as the product of the flapping frequency f and amplitude A (the latter being a length scale similar to the width of the wake), divided by the cruising speed U_0. Physically, the Strouhal number represents the ratio of the flapping characteristic speed fA to the cruising velocity U and is thus related to the mechanical efficiency of the system. Biological swimmers and flyers are found to lie mostly in the range $0.2 \lesssim St_A \lesssim 0.4$ [60; 61]. Another crucial parameter in these problems is the aspect ratio of the flapping body, because it determines to what extent a quasi-two-dimensional (Q2D) view can capture the main elements needed for an adequate description of the real three-dimensional (3D) flow. In particular, in the case of a flapping body propelling itself in forward motion, at least two qualitatively different situations have been evidenced from flapping foil experiments and numerical simulations: high span-to-chord ratio foils produce the aforementioned reverse BvK vortex street [see e.g. 47; 49], where the most intense vortices are aligned with the foil span. A Q2D analysis accounts for the key dynamical features in this case where the mean flow has the form of a jet and results in a net propulsive force. As the span-

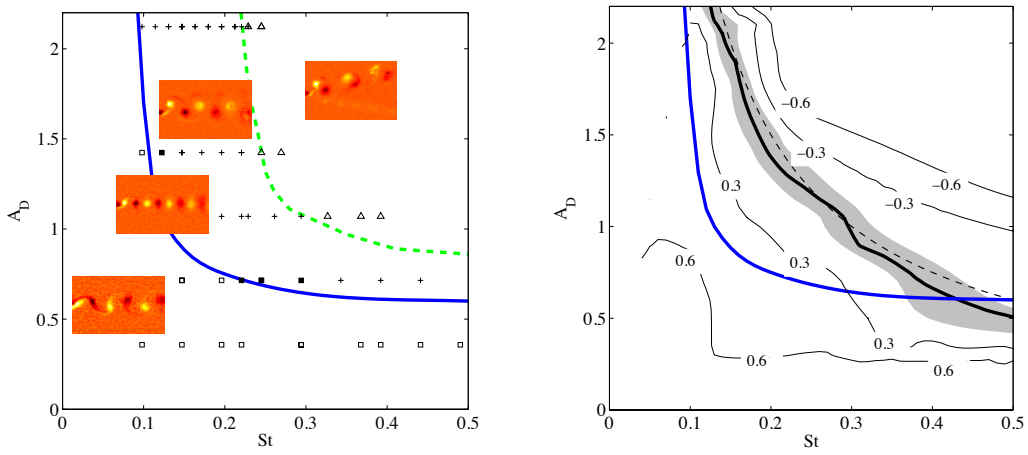

Figure 2.3: Left: Transitions in the wake of a flapping foil in the A_D vs. St map for Re $= 255$ [from 41]. Experimental points are labeled as □: BvK wake; ■: aligned vortices; +: reverse BvK wake; △: deflected reverse BvK street resulting in an asymmetric wake. Solid line: transition between BvK and reverse BvK. Dashed line: transition between reverse BvK and the asymmetric regime. Typical vorticity fields are shown as inserts on each region. Right: Contours of a mean drag coefficient C_D/C_{D0} surface estimated using a momentum-balance approach (here C_{D0} is the drag coefficient for the non-flapping foil at zero angle of attack) [42]. The black line corresponds to $C_D = 0$ where the estimated drag-thrust transition occurs. The shaded area represents the estimated error for the $C_D = 0$ curve due to sensitivity on the choice of the control volume. The blue line is the transition from BvK to reverse BvK reproduced from the left panel. The dashed line corresponds to $\mathrm{St}_A = 0.3$.

to-chord ratio decreases towards unity, 3D effects come into play and modify dramatically the structure of the wake. In this case a series of vortex loops (or horse-shoe vortices) are engendered from the vorticity shed from all sides of the flapping foil [see e.g. 54; 62; 63].

The experiments summarized here were performed with a 4:1 aspect ratio foil, which is high enough to produce Q2D regimes in the near wake. The foil section was chosen with a semi-circular leading edge that defines the maximum width of the foil, narrowing symmetrically to join the trailing edge along straight lines. The geometric simplicity and symmetry of this profile has motivated its use in further studies on the subject of flapping-based propulsion found in the literature [64–66]. Our experimental approach was inspired by the works on vorticity control in the cylinder wake forced by rotary oscillations conducted in previous studies at PMMH [67]. We showed that a two-parameter description that permits to vary independently the frequency and amplitude of the oscillatory motion is the optimum framework to fully characterize the quasi-two-dimensional regimes observed in the wake of a pitching foil. The transition from a BvK vortex street to the reverse BvK street characteristic of propulsive regimes (see Figure 2.2), as well as the symmetry breaking of the reverse BvK street reported in [41; 42] are summarized in the (St, A_D) phase space shown in Figure 2.3 (left). The Strouhal number $St = fD/U_0$ and a dimensionless amplitude $A_D = A/D$ have been defined using a fixed length scale (the foil width D). Note that the product of these two parameters gives the flapping amplitude based Strouhal number from Eq. 2.1 that is often used. One of the main results of obtained form these ex-

periments is that the drag-thrust transition, which we estimated from mean flow measurements, does not coincide exactly with the inversion of the vortex street (see Figure 2.2, right), a fact that is usually assumed in the literature where "thrust-producing wake" is used interchangeably with "reverse Karman wake". In fact, a region in the (St, A_D) plane exists where a reversed BvK pattern can be observed in the wake of the flapping foil, but the relative thrust engendered by the flapping motion is not yet enough to overcome the total mean drag.

2.1.1 Symmetry breaking of the reverse BvK wake

The lateral deflection of the reverse BvK vortex street observed above a certain threshold in the forcing parameter space (above the green dashed line in Figure 2.3, left) was thoroughly scrutinised in these experiments, leading to the establishment of a symmetry breaking criterion [see 41, for details]. The latter is based on the qualitative observation that the deflection of the vortex street results from the formation of a dipolar structure from each couple of counter-rotating vortices shed on each flapping period. Above a certain threshold, the self-advection of the dipolar structure formed over one flapping period is strong enough to decouple from the subsequent vortex in the street and generate a deflection of the mean flow. This mechanism and symmetry breaking criterion have been subsequently verified by other studies [68–71]. The asymmetric wakes occurring in a region of the parameter space that overlaps the high-efficiency Strouhal number range used by flapping animals makes the precise definition of the symmetry-breaking threshold potentially important for the design of artificial flapping-based propulsors and their control.

2.1.2 Effect of the Reynolds number

The Reynolds number dependance of the previous results was only barely mentioned in our initial work. An interesting point is that, although natural vortex shedding exists for the steady flap at these Reynolds numbers (the critical Reynolds number for the flap is approximately 140) even at zero-angle of incidence, no mode competition is observed in the strongly forced flapping regimes studied here. The flapping frequency used to define St is thus equivalent to the main vortex shedding frequency. However, even if for a fixed flapping configuration, i.e. fixed St and A_D, one finds as expected a well defined wake structure, changing the Reynolds number does change the intensity of the vortices, since these are built from the boundary layer vorticity on either side of the foil, which is evidently dependent on the Reynolds number. This is shown in Figure 2.4, where the vorticity field in the wake of the flap for a non-flapping case is compared to a case flapping at $St = 0.25$ and $A_D = 1.42$, a point in the parameter space where a clear reverse BvK street is produced, for various Reynolds numbers. We remark for the non-flapping case (left column in figure 2.4) that small oscillations appear downstream of the flap at $Re = 150$ and a natural BvK vortex street is clearly established from the $Re = 200$ case. In the flapping case, increasing the Reynolds number for fixed St and A_D produces more intense vortices in the wake. We note not only the increasing vorticity of the structures nearest to the symmetry plane, but also that of the filaments connecting opposite signed structures. Particularly in the cases of $Re = 255$ and 305, the filaments can be seen to concentrate producing two outer fringes of vortices with

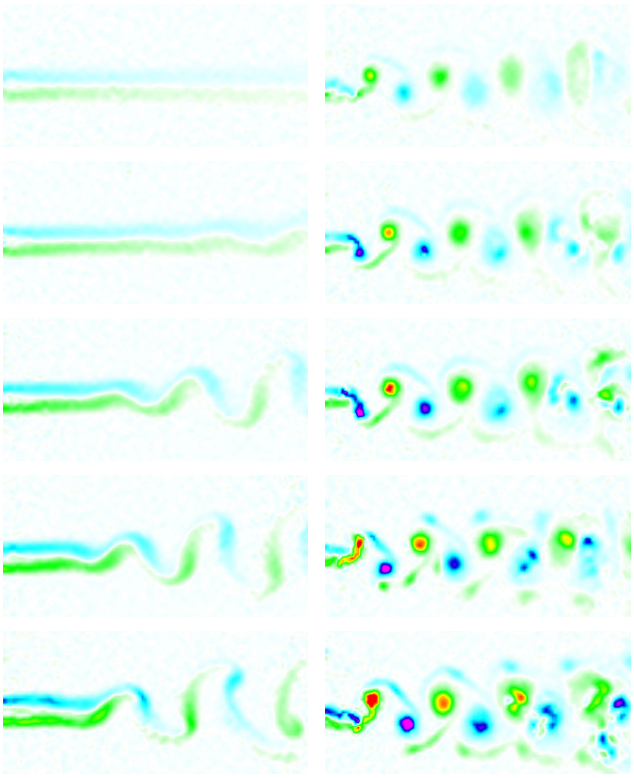

Figure 2.4: Effect of the Reynolds number on the vorticity field in the wake of the foil. Left column: no flapping. Right column: flapping at $St = 0.25$ and $A/D = 1.42$. Values for Re are 100, 150, 200, 255, 305 from top to bottom. [Previously unpublished data]

local maxima weighing up to 30% in absolute value the vorticity of the inner array of vortices at the same horizontal position.

2.1.3 Foil flexibility

As mentioned in the introduction, a major part of our recent work has been devoted to examining model flapping-based propulsion problems in cases where the elastic properties of the propulsive appendage come into play. In the following chapters we will review the problems that we have addressed in a full fluid-structure interaction framework. Before that, the case of the flapping foil in a hydrodynamic tunnel that we have been discussing in the previous sections permitted us to show how adding flexibility plays a strong dynamical role on the wake. We performed a detailed comparison of the vortex dynamics in the near wake of the flapping foil for two cases: the *rigid* foil (our benchmark case which is the foil of our previous studies), and a *flexible* foil with the same shape but made of a compliant material (Figure 2.5).

On the one hand, the effective amplitude obtained passively due to the deformation of the flexible foil while flapping (Fig. 2.5, right) leads to an increase in the propulsive force with respect to the case of the rigid foil [43]. On the other hand, the interaction of the shed vortices

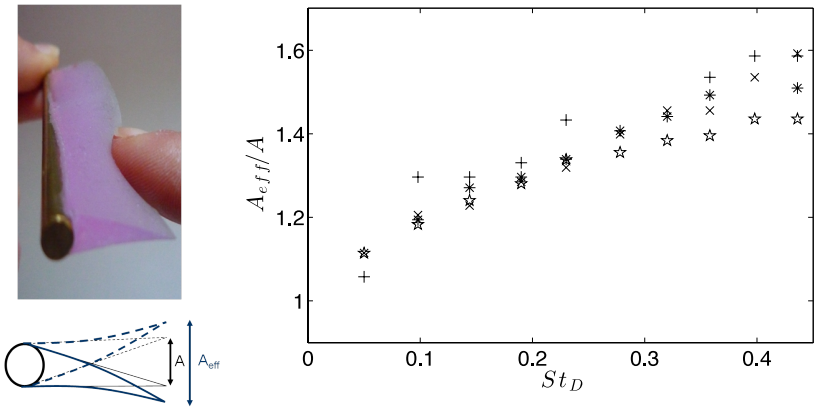

Figure 2.5: Left: Photo of the flexible foil and schematic diagram. Right: Effective flapping amplitude A_{eff} as a function of the Strouhal number $St_D = fD/U$ for θ =5° (+), 7.5° (×), 10° (∗) and 15° (⋆) (which means A_D =0.7 (+), 1.1 (×), 1.4 (∗) and 2.1 (⋆) for the rigid foil).

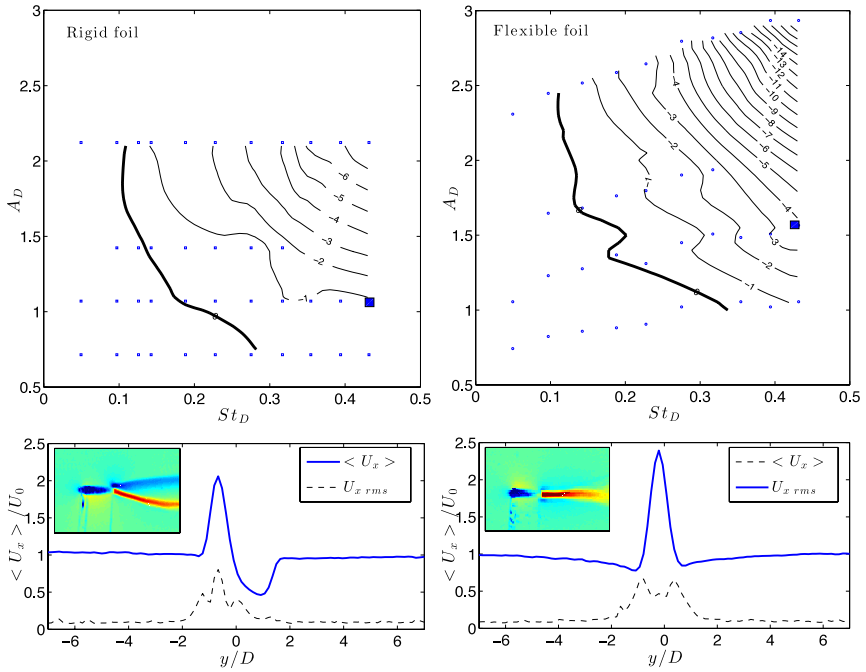

Figure 2.6: Top row: Isocontours of a mean drag coefficient C_D/C_{D0} surface estimated using a momentum-balance approach. The black contour corresponds to $C_D = 0$ where the estimated drag-thrust transition occurs [see 42]. Bottom row: Cross-stream (y) profiles of the mean horizontal velocity on the downstream boundary of the control volume used for the thrust force estimation (solid lines) and corresponding rms (dashed lines) for a typical case (marked with a square symbol in the top plots) where the symmetry breaking is inhibited by the effect of foil flexibility. Insets: Snapshots of the mean $< U_x >$ field showing the jet flow in the wake of the flapping foil.

with the flexible structure inhibits the trigger of the symmetry breaking of the reverse Bénard-von Kármán wake, neutralising thus the deflection of the propulsive jet that has been widely reported in the literature (see Fig. 2.6 and [43]). The latter result evidences that wing compliance needs to be considered as a key parameter in the design of future flapping-propelled vehicles: since not only it is determinant for thrust and efficiency, but also as we show here because of its role in dictating the vortex dynamics that governs the stability properties of the wake.

2.2 Two parallel foils

We close this chapter discussing an experiment based on the same type of flapping foils actuated by a pitching oscillation that we have described above, but in a radically different

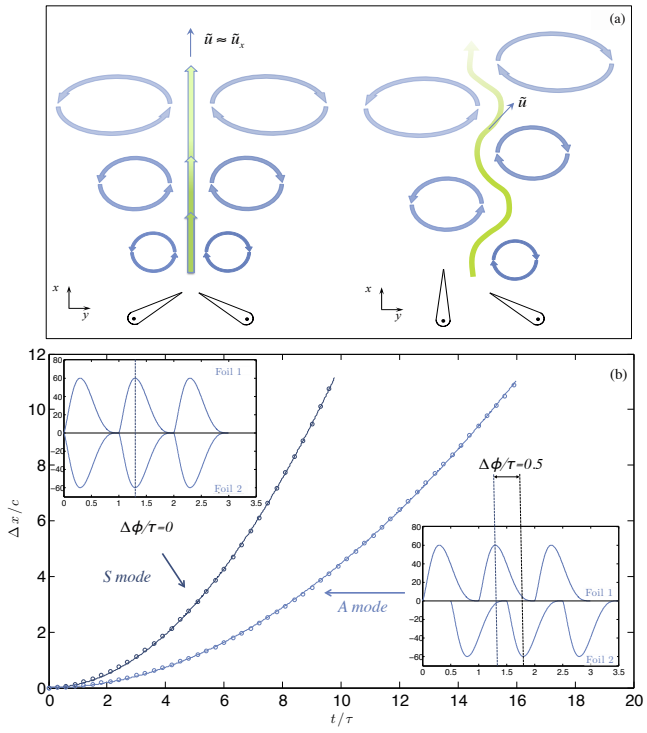

Figure 2.7: (a) Simplified schemes illustrating the topology and velocity fluctuations ($\tilde{\mathbf{u}}$) of the considered wakes. Left: symmetric (*S* mode, jellyfish-like wake) where counter-rotating pairs of vortices are simultaneously shed into the wake. Right: asymmetric (*A* mode, fish-like wake) where counter-rotating vortices are alternatively shed into the wake by the flapping motion. (b) Swimmer's reduced displacement ($\Delta x/c$) for the same distance between foils and forcing frequency in both flapping configurations. Substantially different displacements are achieved from the same momentum input. The driving curves are also shown, the phase lag ($\Delta\phi$) being the only difference between both cases. [Figure from 44]

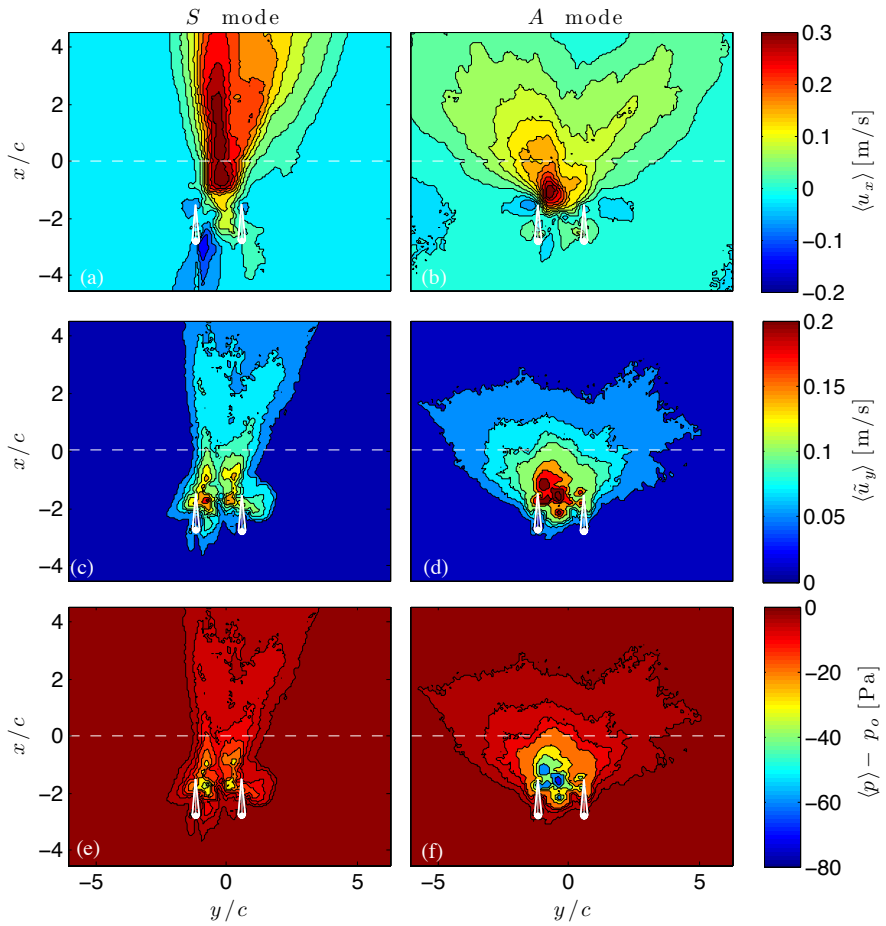

Figure 2.8: (a, b) mean velocity measurements, (c, d) lateral fluctuations of the mean velocity and (e, f) pressure fields calculated from Eq.2.2 for a typical case of the two flapping configurations: Symmetric mode (Left column) and Asymmetric mode (right column).

setup. The idea came from the observation that, depending on the species, propulsive wakes found in nature can differ according to the spatial ordering of the main vortex structures. We used two foils placed in a side-by-side layout to analyse the role of the topology of the wake in the generation of propulsion by comparing two prototypical cases in a quasi-two-dimensional view. One configuration is *jellyfish-like*, with symmetric shedding of vortex pairs, and the other one is *fish-like*, with alternating shedding of counter-rotating vortices (see Figure 2.7). The setup was mounted in a water tank with a free surface in order to support the swimmer by means of an air-bearing rail outside of the water and achieve a self-propelled configuration [see 44, for details]. The crucial point to compare the role of vortex topology in the wake was to provide the same momentum input to produce the two different cases tested. This was carried out by tuning the imposed kinematics as shown in Figure 2.7, where it is also clear that the symmetric mode gives better swimming performance. PIV measurements showing the average velocity

field in the direction of the propulsive jet $\langle u_x \rangle$ and the lateral fluctuations $\langle \tilde{u}_y \rangle$ are displayed in Figure 2.8, together with a calculation of the average pressure field $\langle p \rangle$ derived from the lateral component of the mean Navier-Stokes equation in the turbulent approximation for developing jets (i.e. when the average lateral velocity $\langle u_x \rangle$ and the stream wise gradient of the Reynolds stress are negligible), which reads [72]:

$$\langle p \rangle - p_o = -\rho \left\langle \tilde{u}_y^2 \right\rangle , \tag{2.2}$$

p_o being the pressure away from the wake ($y \to \infty$), where $\left\langle \tilde{u}_y^2 \right\rangle$ is zero. These fields allowed for the calculation of the average propulsive force per unit span $\mathbf{F}_p$, which can be expressed as a simple contribution from the momentum $\rho \langle \mathbf{u} \rangle$ and the pressure $\langle p \rangle$ [73; 74]:

$$\mathbf{F}_p = -\int_{S_e} \rho \langle \mathbf{u} \rangle \langle \mathbf{u} \rangle \cdot \mathbf{n} \, dS - \int_{S_e} \langle p \rangle \mathbf{n} \, dS. \tag{2.3}$$

This very simple experiment allowed us also to identify the physical mechanism behind the better performance of the symmetric mode: a pressure effect related to the intensity of the velocity fluctuations in the near wake [44].

3. *Le petit manège*: a flapping flyer on a merry-go-round

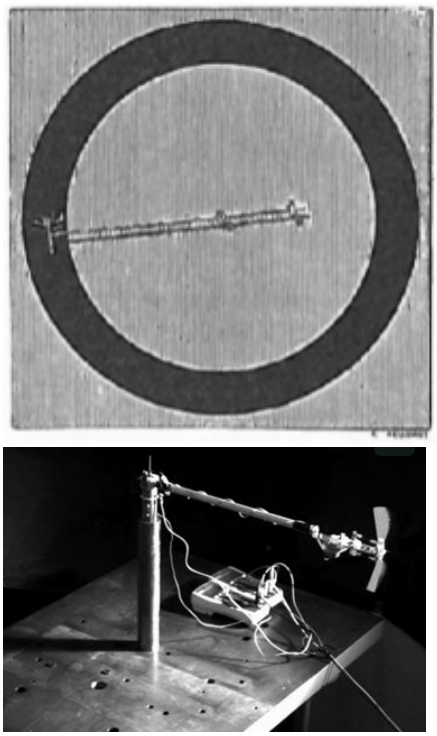

Figure 3.1: Top: Etienne-Jules Marey's petit manège (from [75]). Bottom: PMMH's petit manège

Summary

The work described in this chapter stems from two ideas that developed during our previous work with flapping foils in the hydrodynamic tunnel. We wanted: (1) a system in a self-propelled configuration, and (2) a simpler model to study the effect of wing flexibility on the performance of insect-like flapping wings. The result was the *petit manège* (Fig. 3.1, bottom) inspired by the classic setup conceived by Etienne-Jules Marey to record the kinematics of insect wings (Fig. 3.1, top). We have used this merry-go-round of a flapping device as an experimental platform for a thorough study of the effect of chord-wise flexibility on the performance of flapping wings [76; 77]. Additionally, a modified setup has also served to study the effect of forewing-hindwing interactions in a four-winged flyer.

Collaborators : S. Ramananarivo, M. Centeno, P. Jain, A. Weinreb, B. Thiria

Thiria, Godoy-Diana. *Phys. Rev. E* **82**, 015303R (2010). [76]
Ramananarivo, Godoy-Diana, Thiria. *Proc. Natl. Acad. Sci. USA* **108** (15), 5964-5969 (2011). [77]
Godoy-Diana, Jain, Centeno, Weinreb, Thiria. In *Selected topics of computational and experimental fluid mechanics* (Editors: Klapp et al.) Springer (2015). [78]

3.1 A flexible-wing flyer in a self-propelled geometry

A self-propelled geometry may sound like the evident choice to study a flapping-powered model, but experimentally it brings a certain amount of complications with respect to the usual

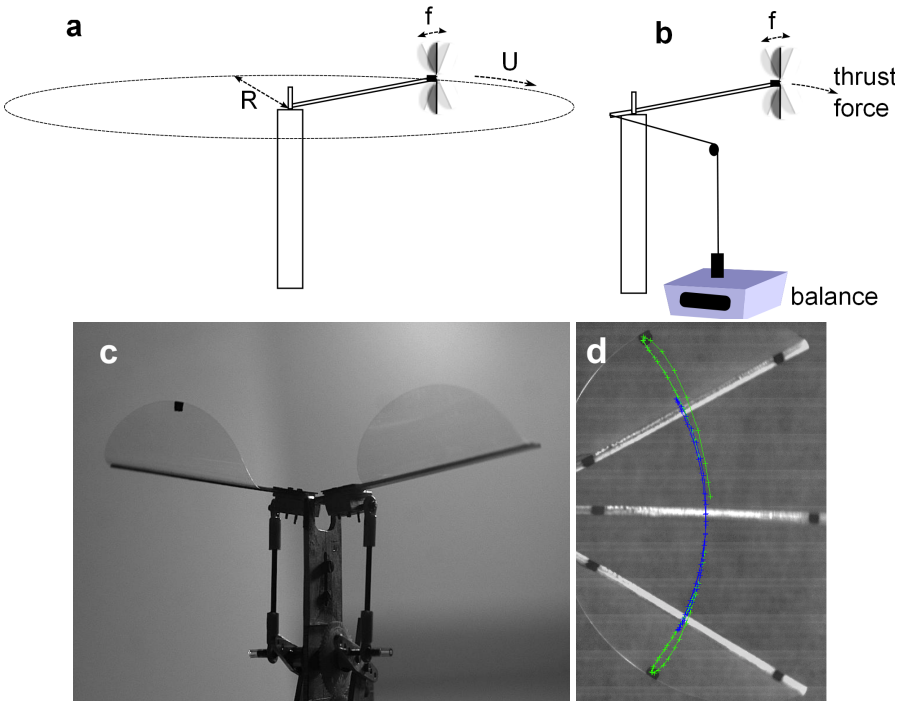

Figure 3.2: Schematic diagram of the flapping flyer in the merry-go-round setup during (a) cruising speed measurement and (b) thrust force measurement [From 76]. (c) Photo of the mechanical "insect" and (d) three instants of the flapping cycle superposed showing the bending wing from a frontal view (in white the leading edge, its tracking in blue; in green the tracking of the trailing edge).

testing facilities (e.g. a wind tunnel or the hydrodynamic tunnel of the previous chapter) where an oncoming uniform flow is driven independently of the flapping motion. [1] In particular, the actuation mechanism has to be mounted on the system that will move relative to the laboratory frame, and power needs to be supplied. The *petit manège* was designed with these requirements in mind, providing a setup (Figure 3.2) enabling measurements of the cruising speed, the thrust force, as well as the consumed power as functions of the imposed wing motion (flapping frequency and amplitude) and wing design. The design of the flyer itself also brought a set of constrains (additional to the choice of materials and actuation), since we wanted a system that performed reasonably well in terms of cruising speed but that remained simple enough to be tractable using basic models for the flexible wing deformation. We found inspiration for the final design of the wings from the literature on insect flight, in particular from Combes & Daniel [13], who showed for a wide variety of insect wings that span-wise flexural stiffness is 1–2 orders of magnitude larger than chord-wise flexural stiffness. We thus opted for wings with a rigid leading edge to focus on chord-wise deformation, and a semi-circular planform was used in order to minimise span-wise bending modes.

1. However, if one thinks of cruising flapping flight, the very fact of decoupling the flapping dynamics and the forward speed makes it difficult also to extrapolate any conclusions about flight performance to the case of a free-flying animal or machine.

3.2 Wing compliance

When considering a flexible wing in the dynamic regime, the forces acting to induce deformation can come from both the fluid dynamic pressure acting on the surface of the wing and the inertial force due to the oscillating acceleration of the wing itself. A measure of the importance of these two bending forces can be given using a simplified model for the flapping wing as a plate of length L, mass surface density μ_s, and bending rigidity B (for a plate of thickness h and Young?s modulus E, $B \sim Eh^3$) whose leading edge is heaving sinusoidally with frequency ω and amplitude A. The moment of the mean fluid pressure force scales then as $M_f \sim \rho_f u_f^2 L^3 = \rho_f \omega^2 A^2 L^3$, where ρ_f is the fluid density and $u_f = A\omega$ is the maximum flapping velocity, whereas the moment of the inertia force scales as $M_i \sim \mu_s L^3 A\omega^2$. The ratio of these two moments $\frac{M_i}{Mf}$ is actually a mass ratio $\frac{\mu_s}{\rho_f A}$, which is greater than 10 for all the wings tested in our experiments [76]. The main bending factor in this case is thus the inertia force, which will be counterbalanced by the elastic restoring force produced by the bent wing. This is consistent with the analysis by [79] who concluded for most wings moving in air that the feedback between fluid pressure stresses and the instantaneous shape of the wing is negligible with respect to the inertial-elastic mechanisms. Comparing the moment of the inertial force M_i to that of the elastic restoring force that scales as $M_e \sim B$, we defined the *elasto-inertial* number [76]

$$\mathcal{N}_{ei} = \frac{\mu_s A\omega^2 L^3}{B} = \left(\frac{L}{L_b}\right)^3 , \tag{3.1}$$

the latter form being expressed in terms of the *bending length* $L_b = (B/\mu_s A\omega^2)^{1/3}$. $\mathcal{N}_{ei}$ measures thus to what extent the inertial force due to the oscillating acceleration will be balanced by the elastic resistance to bending (analog definitions of this bending length arise in problems where other forces drive the bending, see [80; 81] for capillary and hydrodynamical forces, respectively). This definition determines for instance that for $\mathcal{N}_{ei} \ll 1$ the wing is too rigid for the inertia of the oscillating wing to have an observable effect, or in terms of the bending length, $L_b \gg L$ so that no deformation can be observed over the length scale L of the wing chord.

Physically, the form of the bending wing can be seen as a "shape factor" that redistributes the contribution of the aerodynamic forces in both directions –of the flapping motion normal to the wings F_D [1] and of the forward displacement– as sketched in Fig. 3.3. During the flapping motion, the wings experience strong drag as they push fluid up and down during a stroke cycle. Because of the flexibility of the wing, the experienced drag scales on a length depending on L_b [81–83], instead of L as it would for the rigid case. On the other hand, the change in shape induces a contribution of the aerodynamic pressure load in the forward direction that is also dependent on the wing bending.

Interestingly, the elasto-inertial number can also be expressed as a function of the ratio between the forcing and relaxation frequencies times the non-dimensional forcing amplitude of the driving motion, which allows to express directly the bending rate as function of a non-

1. F_D is the drag force that opposes the flapping motion so that in the standard reference frame, where the thrust force is in the direction of the cruising velocity, it is actually a fluctuating lift force, not to be confused with the drag that limits the cruising velocity.

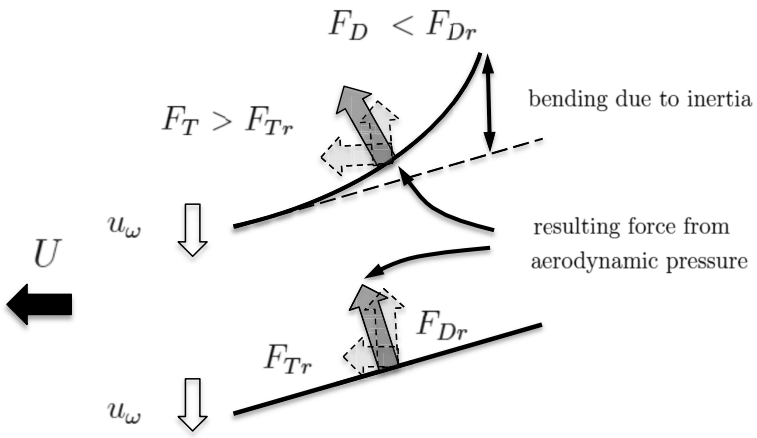

Figure 3.3: Schematic diagram of the redistribution of aerodynamic forces by a bending plate model (top) with respect to a rigid plate (bottom). F_{Tr} is the thrust force and F_{Dr} the drag forces for a rigid wing, respectively. [Figure from 76]

dimensional oscillator forcing term:

$$\mathcal{N}_{ei} = \frac{A_\omega}{L}\left(\frac{\omega_f}{\omega_0}\right)^2 \tag{3.2}$$

an expression therefore useful to explore the nearness of the resonance which we have used to analyze the experimental data obtained with our flapping flyer [77].

The first two plots in figure 3.4 show the raw data for cruising speed and thrust force as a function of the flapping frequency for a series of wings of different thicknesses (and hence bending rigidities). The effect of wing flexibility is readily seen, the most flexible wings performing better, up to a certain frequency where the thrust force and thus also the cruising speed drop. All data can be analysed together using a non-dimensional representation for the thrust power given by the product of the dimensionless thrust force $f_T = F_T L/B$ and cruising velocity $u = U/A_\omega\omega$. The bottom row plots in figure 3.4 show the dimensionless thrust and consumed powers, $p_T = UF_T L/BA_\omega\omega$ and $p_i = P_i L/B\omega$, respectively, as a function of the reduced frequency $\bar{\omega}_f = (\omega_f/\omega_0) = (\mathcal{N}_{ei}L/A_\omega)^{1/2}$. A clear maximum appears in the dimensionless aerodynamic power. Notably, this maximum is located significantly below the structural resonant frequency $\omega_f = \omega_0$. We remark also that there is no sign of a resonant behaviour in the consumed power curve (Fig. 3.4 (d)).

Observations of the wing deformation using high-speed video showed that it is reasonable to consider that the wings bend mostly over the first deformation mode, allowing for a forced-oscillator description where the oscillation of the leading edge is the forcing and that of the trailing edge is the response. Video tracking of the wing deformation was used as shown in Fig. 3.2(d) for the full parameter space, producing data for the non-dimensional amplitude a and phase γ of the response, i.e. of the trailing edge motion in the reference frame moving with the leading edge. Results are displayed in Fig. 3.5 where, in addition to all the experiments in a standard atmosphere, the experiments for the two most flexible wings were also performed

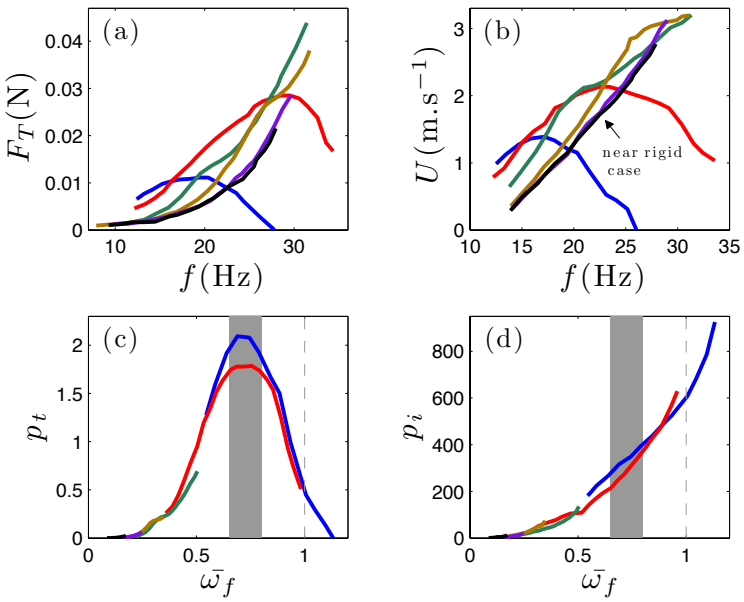

wing thickness, h (mm)	0.050	0.078	0.130	0.175	0.250	0.360
mass per unit area μ_s (kg.m^{-2})	4.50 10^{-2}	10.63 10^{-2}	17.67 10^{-2}	24.12 10^{-2}	34.92 10^{-2}	47.95 10^{-2}
rigidity B (N.m)	3.34.10^{-5}	1.83.10^{-4}	1.02.10^{-3}	2.26.10^{-3}	7.31.10^{-3}	14.00.10^{-3}
relaxation frequency f_0 (Hz)	25.4	34.2	62.2	89.5	117.1	160.8
color label in figures	blue	red	green	yellow	purple	black

Figure 3.4: (a) Cruising speed, (b) thrust force and nondimensional (c) thrust (p_T) and (d) input (p_i) powers as a function of $\bar{\omega}_f$. The gray area represents the optimum region, the dashed line indicates the location of the reduced natural frequency of the wing (linear resonance) [Figure from 77].

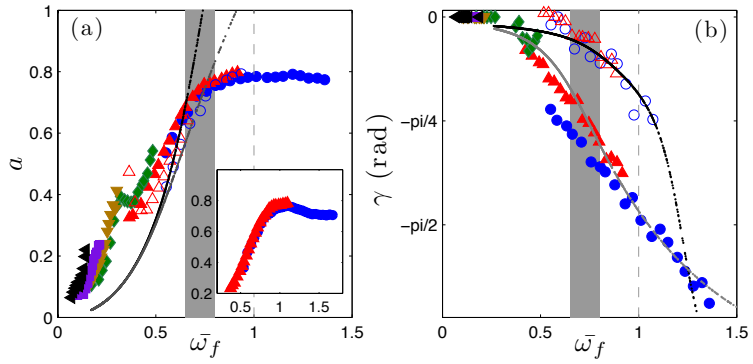

Figure 3.5: Evolution of the non-dimensional amplitude a) and phase b) of the trailing edge wing response as a function of the reduced driving frequency for both flapping amplitudes $A_\omega = 0.8L$ and $A_\omega = 0.5L$ (filled symbols correspond to measurements in air, open symbols in vacuum). Those results are compared to nonlinear predictions from the model in Eq. 3.3 with (gray line) and without (black line) nonlinear air drag [Figure from 77].

in a vacuum chamber at 10 % of the ambient pressure. The latter permitted to test the role of the damping due to aerodynamic drag in the dynamics of the flexible wing. In order to analyse the previous results from a fluid-structure interaction point of view we used a non-linear beam model, i.e. Eq. 1.5 where F_{NL} consists of non-linear terms due to inertia and curvature and $\mathcal{F}_{f/s}$ is a quadratic damping term to account for aerodynamic drag. Introducing a new dimensionless variable $w(x,t) = (h(x,t) - W(t))/L$ to describe the system in the reference frame of the leading edge the beam equation reads:

$$\overbrace{w'''' + \ddot{w}}^{\text{Linear beam}} = \overbrace{-(w'w''^2 + w'''w'^2)'}^{\text{Curvature non-linearity}} \overbrace{- \frac{1}{2}\left[w' \int_1^x \frac{\partial^2}{\partial t^2}\left[\int_0^x w'^2 dx\right] dx\right]'}^{\text{Inertial non-linearity}} \overbrace{-\xi \dot{w}}^{\text{Linear damping}} \overbrace{-\xi_{nl}|\dot{w}|\dot{w}}^{\text{Quadratic damping}} \overbrace{- \frac{A_\omega}{L}\ddot{W}}^{\text{Inertial forcing}} \tag{3.3}$$

Keeping only the first mode of an expansion of the displacement as $w(x,t) = \sum_1^\infty X_p(t)\Phi_p(x)$ (where Φ_p are the non-dimensional *linear* modes for clamped-free beams) and using a classical multiple scales method [see details in 77], the amplitude a and phase γ of the oscillation of the trailing edge can be obtained (lines in Fig. 3.5).

The main observations from Fig. 3.5 are the following: (1) the amplitude of the response increases rapidly with frequency, which is readily explained by the inertial forcing to the system (last term in Eq. 3.3), until it saturates because of the geometric limitation imposed by the finite chord length of the wing. Measurements in air and vacuum are approximately the same, in accordance with the hypothesis stated above that solid inertia is the main bending factor. (2) No clear resonance is observed around $\bar{\omega}_f = 1$ at these large-amplitude oscillations —only a barely visible peak is observable when testing a lower flapping amplitude as shown in the insert in Fig. 3.5(a). A slight but rather broad peak can nonetheless be observed in the nearness of $\omega_0/3$ in the amplitude curve, which can be explained as a super-harmonic resonance consequence of the cubic nonlinearities in Eq. 3.3 [see 77]. (3) Concerning the phase γ, the present results recover the trend of what has been reported previously in the literature [84–87]: $|\gamma|$ increases monotonically with $\bar{\omega}_f$. A remarkable point is that, contrary to what we have noted for the amplitude a, there is a large difference in the evolution of the phase γ between the case in vacuum and that in air at atmospheric pressure: It is clearly observed that γ decreases more slowly in the low density environment within the whole range of flapping frequencies studied. From the beam model point of view, this shows that the quadratic damping term due to aerodynamic drag is responsible for the rapid phase lag observed when increasing the flapping frequency. Now, considering together the performance increase in the first part of the aerodynamic power curve $p_t(\bar{\omega}_f)$ (Fig. 3.4(c)), and the corresponding increasing phase lag, supports the idea of a more favourable repartition of the aerodynamic forces by the bent wing sketched in Fig. 3.3. Indeed, as γ increases the wing experiences a larger bending at the maximal flapping velocity where the beneficial effect of bending the wing is most useful. Connecting the phase dynamics to the propulsive performance has been done in other configurations [85; 86] and it would mean that

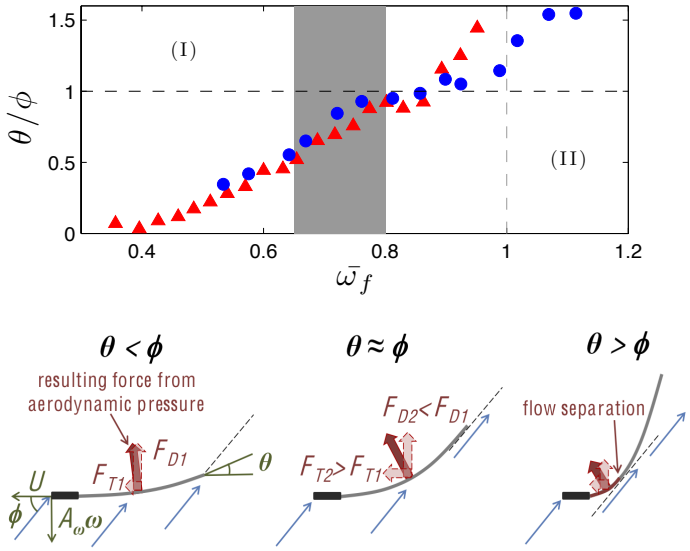

Figure 3.6: Evolution of the two characteristic angles of the wing motion θ and ϕ as a function of the reduced driving frequency $\bar{\omega}_f$. Two regimes can be distinguished: (I): $\phi < \theta$ corresponding to the performances increasing stage due to a useful phase lag. (II): $\phi > \theta$ corresponding to the transition to under-performances due to a loss of the effective wing area. The optimum occurs therefore when ϕ and θ point at the same direction (best phase lag). [Figure from 77]

the thrust power should increase with the phase lag until the point where the wing experiences its largest bending at $\gamma = \pi/2$, a point from which further increasing the phase lag would be counter-productive. However, while the previous argument can explain the initial trend of the performance curve in Fig. 3.4(c), it is clear that the maximum performance does not actually occurs at the expected $\gamma = \pi/2$, but relatively far below at around $\gamma \sim \pi/4$.

Examining the wing deformation kinematics we showed that the optimum is actually ruled by an aerodynamic constrain: the previous argument for the theoretical optimal value $\gamma = \pi/2$ is only valid if the surrounding flow is totally attached to the wing (i.e. if separation occurs only at the trailing-edge). A measure of the susceptibility to separation from the kinematics is given by the ratio of the effective angle of attack at the leading edge ϕ (equivalent to the advance ratio in propeller theory, see also [88, part III] and [89]) to the angle of the tangent to the wing at the trailing edge θ. A situation where $\theta > \phi$ is strongly subjected to flow separation before the wing trailing edge. In this case the effective surface relative to the aerodynamic load can be expected to be drastically reduced leading to a loss of aerodynamic performance (see Figure 3.6).

Summarizing, the instantaneous wing shape is given by the two following ingredients: Inertia provokes the bending (gives the amplitude) and damping, by controlling the phase lag, allows this bending to be usefully exploited. From there, the aerodynamic mechanism described in Fig. 3.6 determines the limit of the beneficial effect of bending.

3.3 Four-winged flyer

From a biological point of view, the case of four-winged flyers capable of out-of-phase motion between forewings and hindwings such as dragonflies is particularly interesting. In the words of [90]: "Dragonflies can hover, fly at high speed and maneuver skillfully in the air in order to defend their territory, feed on live prey and mate in tandem formation". Forewing-hindwing phase-lag has been shown in hovering configurations to be determinant for flight performance [91]: optimal efficiencies have been found for out-of-phase beating whereas in-phase motion of forewings and hindwings has been shown to produce stronger force [92; 93]. The physical mechanisms behind these differences in performance have nonetheless not yet been completely elucidated, and open questions remain in particular when considering the role of wing elasticity. Wing deformation is important because it can passively modify the effective angle of attack of a flapping wing, determining thus its force production dynamics. We have used a modified version of our mechanical insect with two pairs of wings (Figure 3.7) to address these questions experimentally.

The two wings are driven by a single direct-current motor with a set of gears that allows to fix the phase difference between the forewings and the hindwings. All wings beat thus at the same frequency which was varied between 15 and 30 Hz. We have reduced the parameter space in the experiments reported here by fixing the physical characteristics of the flyer. Namely, the distance between the wings d, the stroke amplitude θ_0 and the chord-wise flexural rigidity of the wings. It should of course be noted that these parameters in the present tandem wing configuration, in particular the wing spacing d, should in general be analysed simultaneously with the forewing-hindwing phase lag [91; 94]. The motion of the wings is described using the angles of the forewing and hindwing leading edges in the flapping plane, θ_{fw} and θ_{hw}, respectively, as

$$\theta_{fw} = \theta_0 \sin(2\pi f t) \text{ and } \theta_{hw} = \theta_0 \sin(2\pi f t - \varphi) , \tag{3.4}$$

where f is the flapping frequency and the phase lag φ is varied between 0 and 2π. For $0 < \varphi < \pi$ the forewing is leading whereas for $\pi < \varphi < 2\pi$ it is the hindwing that leads. The Reynolds number $\mathrm{Re} = Uc/\nu$ based on the cruising speed and the chord length was in the range of 1000 to 4000.

The performance results are summarised in Fig. 3.8. In the first frame U is plotted in

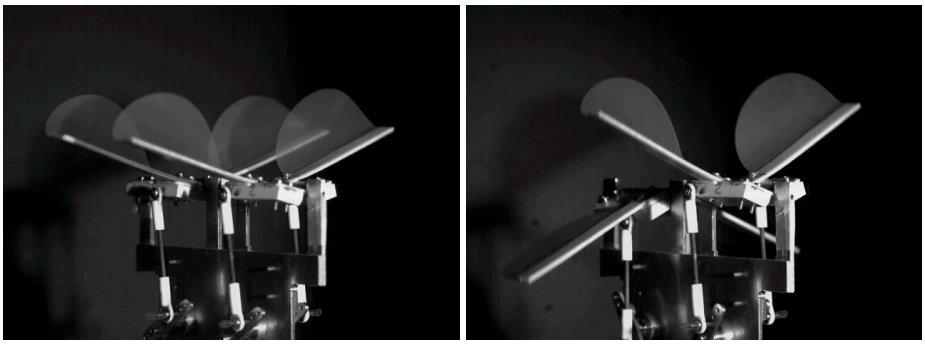

Figure 3.7: Photos of the flapping flyer with forewing-hindwing phase lags 0 (left) and π (right).

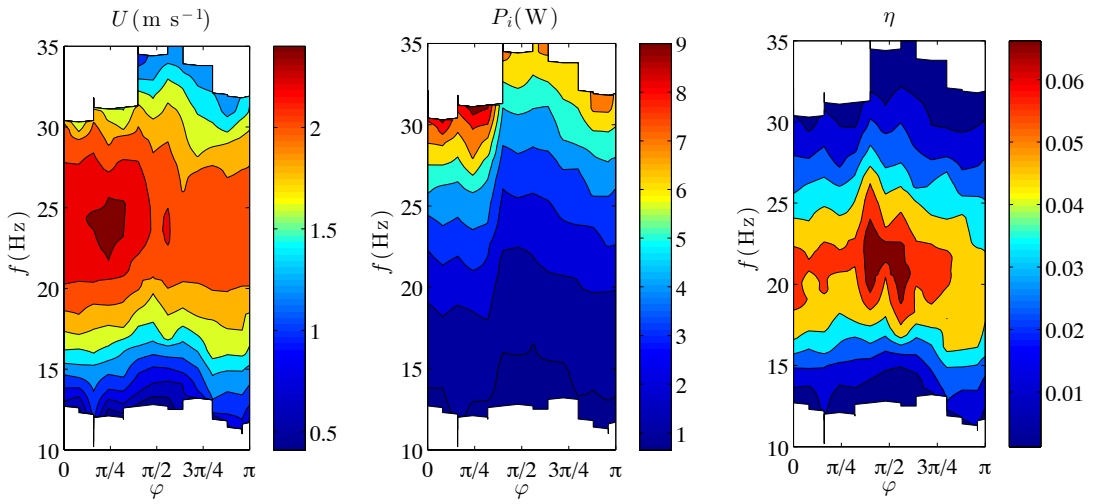

Figure 3.8: Cruising speed, consumed power and efficiency (see text) as a function of the forewing-hindwing phase lag and the flapping frequency. Only the first half o the phase-lag φ range where the forewing is leading was examined here.

coloured contours in a (φ, f)-space for $\varphi \in [0, \pi]$ and scanning the full range of flapping frequencies available experimentally. For all phase lags, a clear maximum of the attained cruising speed occurs always around 24Hz (the optimal frequency can be expected to be dictated by the elastic properties of the wings). The second plot in Fig. 3.8 shows the consumed power P_i in the same parameter space. Here the main observation is that, while not surprisingly consumed power increases monotonically with increasing flapping frequency, phase lag plays an important role for energy expenditure, regardless of the flapping frequency. We use the two previous measurements to define the following expression of efficiency, considering that the aerodynamic thrust power is proportional to U^3 (velocity times thrust force, the latter being $\sim U^2$):

$$\eta = \frac{\frac{1}{2}\rho S U^3}{P_i} \tag{3.5}$$

where S is the effective wing surface. Other definitions of efficiency using purely dynamical parameters [e.g. 95] should give equivalent results to the expression 3.5 chosen here in terms of the measured consumed power P_i. It can be seen that the optimum in terms of efficiency is shifted toward larger phase lags (around $\varphi \approx \pi/2$) than the optimum in terms of maximum cruising speed [More details in 78].

4. Playing with *Pieris rapae*

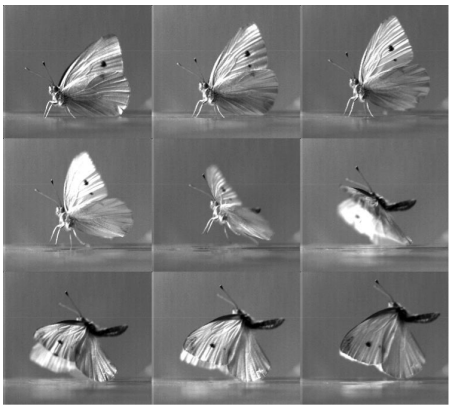

Figure 4.1: Successive stages of the butterfly take-off over half wingbeat period [From 96].

Summary

The present chapter reviews a project that emerged from the collaboration with Jérôme Casas' group at IRBI in Tours. We used the small white cabbage butterfly *Pieris Rapae* to study the take-off maneuver, which remains an elusive phase of insect flight relatively poorly explored compared to other maneuvers. Focusing on the first downstroke, we have addressed the different mechanisms involved in the force production during take-off from a force balance perspective, in butterflies taking-off from the ground. In order to determine if the sole aerodynamic wing force could explain the observed motion of the insect, we have firstly compared a simple analytical model of the wings force to the acceleration of the insect's center of mass estimated from video tracking of the wing and body motions. Secondly, the wing kinematics has also been used for numerical simulations of the aerodynamic flow field. Similar wing aerodynamic forces were obtained by the two methods. Both are however not sufficient, nor is the inclusion of the ground effect, to predict faithfully the body acceleration. We have to resort to the legs forces to obtain a fitting model. We show that the median and hind legs display an active extension responsible for the initiation of the upward motion of the insect's body, occurring before the onset of the wing downstroke. We estimate that legs generate, at various times, an upward force which can be much larger than all other forces applied to the insect's body. The relative timing of leg and wing forces explain the large variability of trajectories observed during the maneuvers.

Collaborators : G. Bimbard [1]*, D. Kolomenskiy, J. Casas*

Reference :

Bimbard, Kolomenskiy, Bouteleux, Casas, Godoy-Diana *J. Exp. Biol.* **216**, 3551-3563 (2013) [96].

1. This work was part of Gaëlle Bimbard's PhD project at IRBI.

4.1 Take-off force balance

We focus on the first downstroke of Pieris rapae (Lepidoptera: Pieridae) butterflies taking off from a horizontal flat surface. Starting from a natural position prior to take-off with both wings pointing upwards, the first downstroke starts producing the lift force that drives the ground-to-air transition (see Fig. 4.1). A high-speed video recording setup with three cameras (see Fig. 4.2) was used to record spontaneous take-offs, giving access to time-resolved wing and body kinematics. In particular, tracking of the centre of mass of the insect was used to test the simple balance of forces in the vertical (z) direction:

$$m\ddot{z}_{\mathrm{cm}} = F_z(t) - mg\ , \tag{4.1}$$

in terms of the position z_{cm} of the centre of mass of the insect, its mass m and the gravitational acceleration g. The upward force $F_z(t)$ can thus be calculated from the measured position $z_{\mathrm{cm}}(t)$ and used to elucidate the mechanisms of of force production during take-off.

Considering first the aerodynamic force, at $t = 0$ the butterfly is on the ground and as the wings start moving downwards they will produce a lift force. We attempted first to compare a

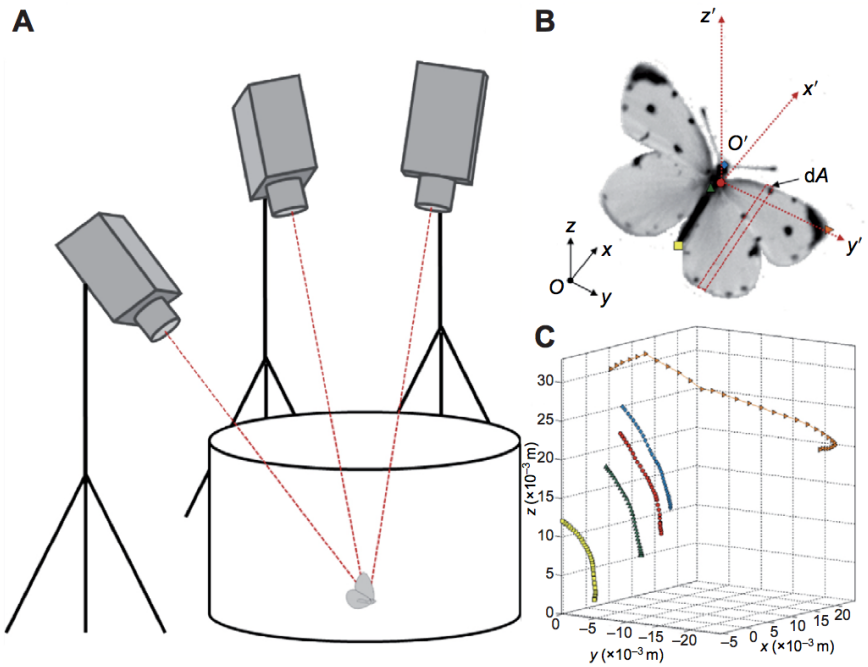

Figure 4.2: (A) Video recording setup. (B) Reference frames and definition of the points used for the video tracking. $Oxyz$ is the frame fixed on the earth; $O'x'y'z'$ is the frame fixed on the wing, with its origin at the wing root. The $y'-$axis, along which wing elements of various area dA follow each other, spans the wing from the root (red circle) to the tip (orange triangle). The blue diamond, the green triangle and the yellow square represent the head, the center of mass and the tip of the abdomen of the insect, respectively. (C) Tracked points in the $Oxyz$ reference frame for the first half wing beat [From 96].

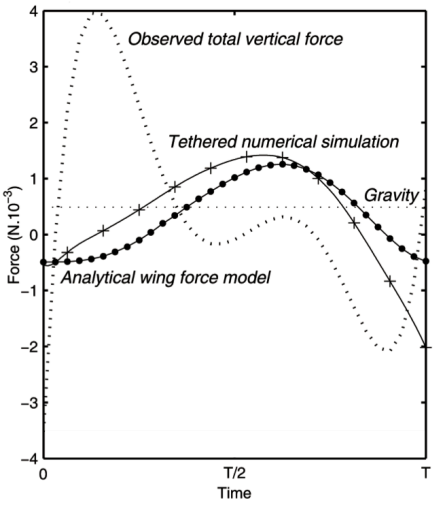

Figure 4.3: Evolution of the net vertical forces produced during take-off flight for one case. The dotted line represents the evolution of the total vertical force actually acting on the insect ($m\ddot{z}$) while the solid curve punctuated by points symbolises the analytical wing force model $F_z^{am}(t)$, calculated using Eq. 4.2. The black line punctuated by crosses represents the tethered numerical simulation [From 96].

rough estimate of the force produced by the wings during the first half wingbeat period to the acceleration of the actual force $F_z(t)$ calculated from the motion of the centre of mass.

For each wing, we consider the dynamic pressure $\rho|\vec{u}|^2$, where ρ is the fluid density and $\vec{u}$ is the instantaneous velocity acting on an element the area dA of the wing (Fig. 4.2B). It produces a force d$\vec{F}$ that is oriented at each instant in the direction normal to the wing surface. Using for each wing a reference frame with the origin at the wing base, chosen so that one of its axes is aligned with the plane of motion during the first half wingbeat period (see y-axis in Fig. 4.2B). Furthermore, the velocity of a slice of wing element can be written $u = y'\dot{\theta}$, considering a wing surface described by a chord that varies along the span as the function $c(y')$. Here $\dot{\theta}$ is the angular velocity of the wing, i.e. $\theta(t)$ is the angle describing the wing motion (and the direction of the y'-axis), which is obtained from the kinematics measurements. The element of force projected in the direction of gravity can be thus written $\mathrm{d}F = 2\rho y'^2\dot{\theta}^2 c(y')\cos\theta\cos\gamma\mathrm{d}y'$, where γ is the angle between the x'-axis and the horizontal (see Fig. 4.2B) and where the element of area of the wing $\mathrm{d}A = c(y')\mathrm{d}y'$ is written in terms of the chord $c(y')$. Integrating along the wing span gives the lift force as a function of time

$$F_z^{am}(t) = 2\rho\dot{\theta}^2(t)\cos\theta(t)\cos\gamma\int_0^{\text{span}} c(y')y'^2\mathrm{d}y' \,. \tag{4.2}$$

The output of this rough model was not able to explain the upward force values $F_z(t)$ from the centre of mass motion measurements, hinting to the necessity of including other sources of force. Numerical simulations of the aerodynamic flow field using the wing kinematics were carried out for flight setups assuming tethered and free flight conditions, and with or without the presence of the substrate to test for the ground effect [see details in 96]. The simulations showed

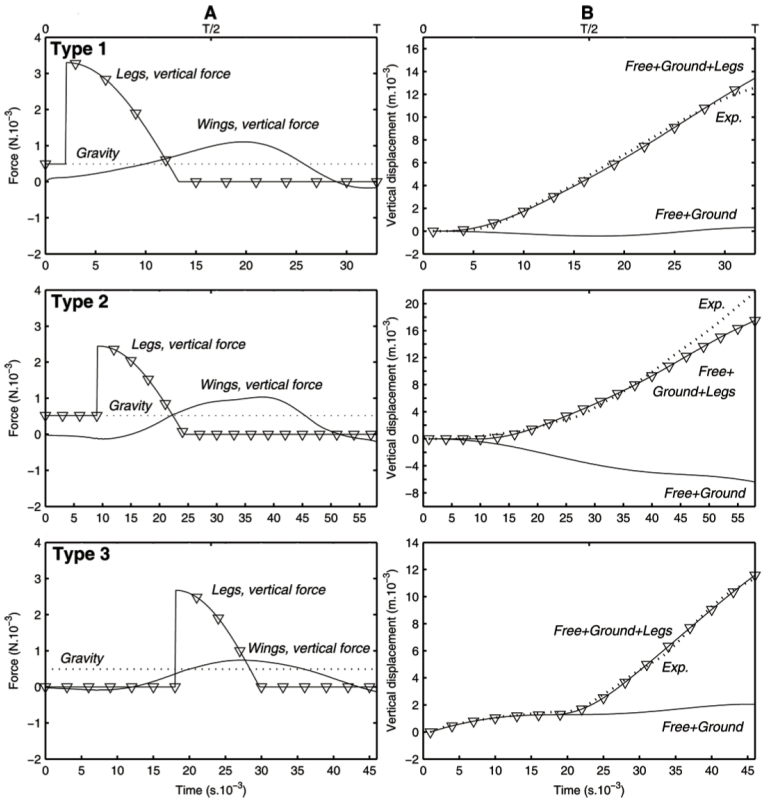

Figure 4.4: Legs forces and forces integration from numerical simulations three types of take-offs. **Column A**. Time evolution of the vertical forces acting on the insect's body during the three different types of take-offs. The vertical components of the force generated by the legs model and of the total aerodynamic force of the two wings obtained in the free/ground numerical simulation are shown. The gravity force mg is also represented for reference. **Column B**. Time evolution of the vertical position of the insect's centre of gravity. The downstroke time in milliseconds is also shown here for each take-off type. [From 96].

that the global trend of the aerodynamic force was relatively well predicted by the previous rough model (see Fig. 4.3) and also that the ground effect played only a minor role (mainly because of the transient nature of the take-off maneuver). We thus showed that the leg extension has to be taken into account as one of the main elements in the take-off force balance. The lift force in Eq. 4.1 can thus be written $F_z(t) = F_{az} + F_{lz}$, where F_{az} and F_{lz} are the forces produced by the wings and the legs, respectively. Using a linear compression spring model for F_{lz}, we proved that these legs forces can be active from the very beginning of the maneuver or at the same time as the peak of aerodynamic lift, in the second portion of the first downstroke (see Fig. 4.4 and [96]).

5. Undulatory swimming

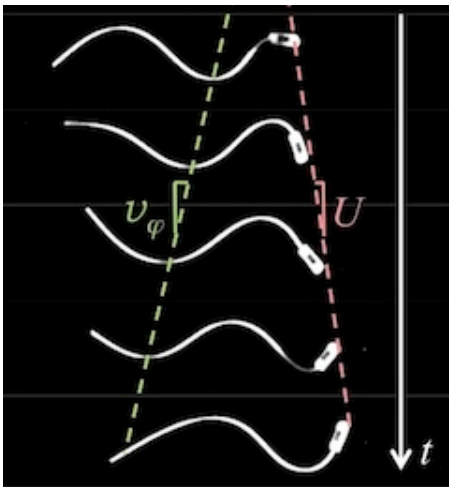

Figure 5.1: Snapshots of an undulating swimmer defining the cruising speed U and the phase velocity v_φ of the body undulation.

Summary

Swimmers in nature use body undulations to generate propulsive and manoeuvring forces. The undulatory kinematics is driven by muscular actions all along the body, involving a complex temporal and spatial coordination of all the local actuations. Such swimming kinematics can be reproduced artificially, in a simpler way, by using passively the elasticity of the body. Here we present experiments using this idea with self-propelled elastic swimmers in the inertial regime. The first experiment is based on magnetically-actuated self-propelled swimmers on a free surface [97]. By addressing the fluid-structure interaction problem of undulatory swimming, we show that our artificial swimmers are well described by coupling a beam theory with the potential flow model of Lighthill [29]. In particular, we show that the propagative nature of the elastic wave producing the propulsive force is strongly dependent on the dissipation of energy along the body of the swimmer [98]. In the second experiment we use rectangular flexible foils forced by a rotational oscillation at one extremity and allowed to self-propel along a fixed direction, enabling the discussion of the problem of drag on an undulating self-propelled swimmer [99]. The foil experiment was then used to discuss the interaction of a swimmer with a solid boundary (see [100] included in the appendix).

Collaborators : S. Ramananarivo, V. Raspa, M. Piñeirua, R. Fernández-Prats, F. Huera-Huarte, B. Thiria

References :

Ramananarivo, Godoy-Diana, Thiria *J. Roy. Soc. Interface* **10**, 20130667 (2013). [29]
Ramananarivo, Godoy-Diana, Thiria. *EPL*, **105**, 54003 (2014). [98]
Raspa, Ramananarivo, Thiria, Godoy-Diana. *Phys. Fluids*, **26**, 041701 (2014). [99]
Ramananarivo, Thiria, Godoy-Diana. *Phys. Fluids*, **26**, 091112 (2014) *Gallery of Fluid Motion. [97]
Fernández-Prats, Raspa, Thiria, Huera-Huarte, Godoy-Diana. *Under review* (2014). [100]

5.1 Lighthill's elongated body theory

In order to describe the production of a propulsive force by an undulatory swimmer one can think of the sum of the contributions of each section of the undulating body. In the inertial regime, two main physical ingredients have to be considered: (1) the hydrodynamic drag and (2) the acceleration reaction, both acting on each section of the swimmer's body. These two ingredients have been formalised giving rise, respectively, to Taylor's *resistive* theory [101] and Lighthill's *reactive* theory [102]. The former case is a quasi-static model, where the instantaneous force is determined at each time by the value of the instantaneous velocity of the section of the body —hence not considering the effect of acceleration—, and in that sense it resembles the theoretical framework describing low-Reynolds-number swimmers [103], excepted that the friction force opposing the lateral displacement of each body section is not linear but quadratic. In the reactive model on the contrary, lateral forces come from the reaction force following the acceleration that the body motions have given to the surrounding fluid, and they can thus be described by a potential flow theory. The latter model has been the most widely used to describe large-Reynolds-number swimmers, however, for realistic modelling purposes it has been customary to couple it to additional models that account for viscous effects, bringing in practice the resistive theory back into play [see e.g. 104].

We recall briefly here the main points of Lighthill's reactive theory, which we have used to describe our artificial self-propelled swimmers. Lighthill showed that the estimation of the thrust force only requires the knowledge of the local kinematics at the tail of the deformable body [see also 17; 31; 105]. In the small lateral displacement approximation, the mean thrust force $\overline{T}$ can be written in terms of the local deflection of the slender body with respect to the axis of swimming $h(x,t)$ as:

$$\overline{T} = \frac{m}{2}\left[\overline{\left(\frac{\partial h}{\partial t}\right)^2} - U^2\overline{\left(\frac{\partial h}{\partial x}\right)^2}\right]_{x=L}. \tag{5.1}$$

where m is the added (or virtual) mass of fluid, which can be written for a slender swimmer as $m = \rho S$ (with ρ the fluid density, and S the swimmer cross-section). The subscript $x = L$ means that the derivatives in Eq. 5.1 are evaluated at the tail. This expression of the force is obtained by writing that the swimming power $\overline{T}U$ (i.e. the product of the thrust force times the swimming velocity) corresponds to the rate of working $\overline{W}$ done by the fish through its lateral forces (i.e. the integral of the work done by the instantaneous lift per unit length in making a displacement $h(x,t)$ at a rate of $\partial h/\partial t$), minus the rate of shedding of the kinetic energy associated with lateral fluid motion, which can also be expressed in terms of the derivatives of $h(x,t)$. This swimming energy conservation then reads:

$$\overbrace{\overline{T}U}^{\text{swimming power}} = \overbrace{\overline{W}}^{\text{muscle power}} - \overbrace{\frac{m}{2}\overline{\left[\frac{\partial h}{\partial t} + U\frac{\partial h}{\partial x}\right]^2}_{x=L} U}^{\text{rate of shedding of kinetic energy}}. \tag{5.2}$$

The part corresponding to the energy transferred to the fluid can be seen as a source of dissipation for the mechanics of the swimming fish, as this energy is lost into the flow and will not be used

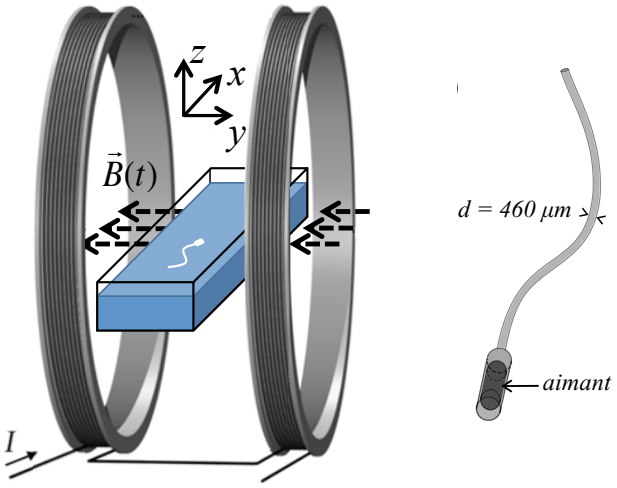

Figure 5.2: Experimental setup (Left): a water tank is placed inside a Helmholtz coil pair. Right: schematic diagram of the flexible swimmer with the magnet embedded at its head [Figure from 2].

for sustaining the body deformation. Together with its large-amplitude version [106], this theory has been extensively used in the literature as mentioned above, although only recently extended to a three-dimensional framework and confirmed using numerical simulations [107].

The question of efficiency can be also addressed within this framework defining it as the ratio between the propulsive power to the muscle power [102]:

$$\eta = \frac{\overline{T}U}{\overline{W}} = 1 - \frac{1}{2}\left(\frac{\partial h}{\partial t} + U\frac{\partial h}{\partial x}\right)^2\Bigg|_{x=L} \Bigg/ \overline{\frac{\partial h}{\partial t}\left(\frac{\partial h}{\partial t} + U\frac{\partial h}{\partial x}\right)}\Bigg|_{x=L}, \tag{5.3}$$

which measures the ability of the swimmer to produce useful propulsive power from the work exerted by its body motions.

5.2 Elastic filament swimmer on a free surface

We present now our experimental setup with self-propelled swimmers on a free surface. The swimmers, modelled as flexible thin filaments, are composed of a cylindrical body of diameter d 0.5mm made of a flexible polymer (polyvynil syloxane), with a small embedded magnet constituting the head. They float through capillary forces at the free surface of a water tank. A time-varying but spatially-uniform magnetic field is generated using a Helmholtz pair of coils powered by an AC voltage. The field actuates the head of the swimmer by producing an oscillating magnetic torque as the permanent magnet attempts to align with the alternating field. The rotational oscillations of the magnet generate a backward-propagating wave along the flexible tail, causing it to swim forward. Fig. 5.2 shows schematically the experimental setup and the geometry of the swimmer. Fig. 5.3 presents snapshots of a swimmer a 5cm long swimmer with its head oscillating at 13Hz where the wake is visualised by colouring the body of the swimmer with fluorescein dye prior to starting the experiment.

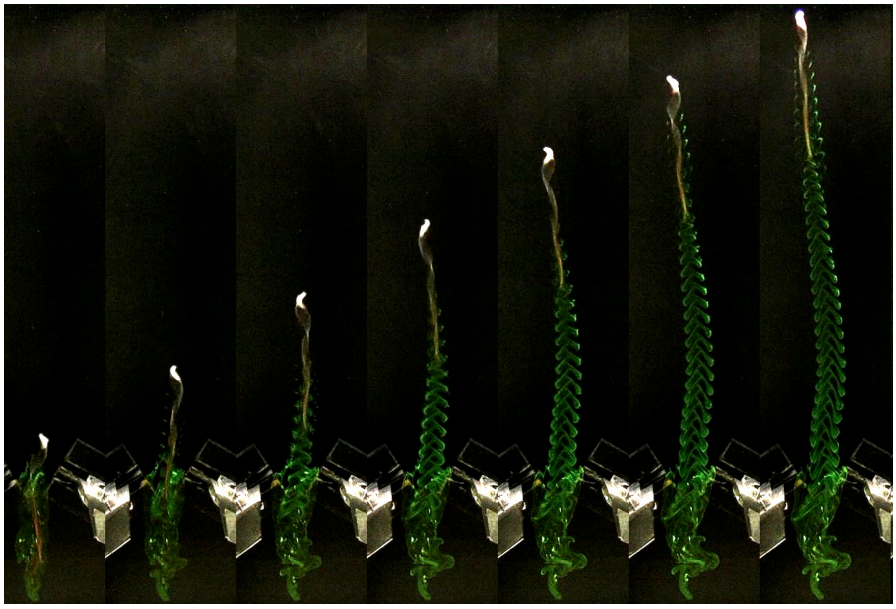

Figure 5.3: Flourescein-dye visualisation of the wake of an elastic swimmer on a free surface. From left to right, snapshots every 0.5 s are shown [Figure from 97]. [See video in URL: http://vimeo.com/77356211]

We have followed two ideas to understand the dynamics of these artificial swimmers: on the one hand, we resort to the fluid-structure interaction framework discussed previously (Eq. 1.5) to describe the deformation of the flexible filaments subjected to the actuation at one extremity. The crucial finding on this line has been that the propagative nature of the elastic wave that mimics the anguilliform kinematics is strongly dependent on the energy dissipation along the body of the swimmer due to fluid damping [29; 98]. On the other hand, we have coupled the thrust estimation from Lighthill's theory for slender fish swimming (Eq. 5.1) with a global drag model, in order to describe the self-propelled regime where the final cruising swimming speed U is determined by a balance between the forward thrust generated by the body undulations and the drag experienced by the filament.

Considering the first point, the resulting beam equation now reads:

$$\overbrace{(1+\tilde{m})\ddot{y}+y''''}^{\text{Linear beam with added mass}} + \overbrace{\tilde{m}\left[2\tilde{U}\dot{y}'+\tilde{U}^2y''\right]}^{\text{“Flag” terms}} + \overbrace{\tilde{\alpha}\left|\dot{y}+\tilde{U}y'\right|(\dot{y}+\tilde{U}y')}^{\text{Quadratic dissipation}} = 0\,, \tag{5.4}$$

which is written in dimensionless variables [1] and differs from the case of Chapter 3 for the model of the insect wing in that: (1) the effect of added mass term is now non negligible, (2) a potential flow model for the surrounding fluid brings two extra terms that depend on the swimming velocity (labelled "flag" terms in the equation since they are responsible of the flapping flag instability when an outer flow of sufficient velocity is imposed, see e.g. [108]), and (3) because smaller

1. $\tilde{U}=UL\sqrt{\mu/B}$ is the reduced velocity, $\tilde{m}=M/\mu$ the mass ratio and $\tilde{\alpha}=\frac{1}{2}\rho dC_dL/\mu$ the non-dimensionalized damping coefficient. Note that $\tilde{\alpha}$ depends on L, which reflects the increasing effect of damping when the filament is longer [29].

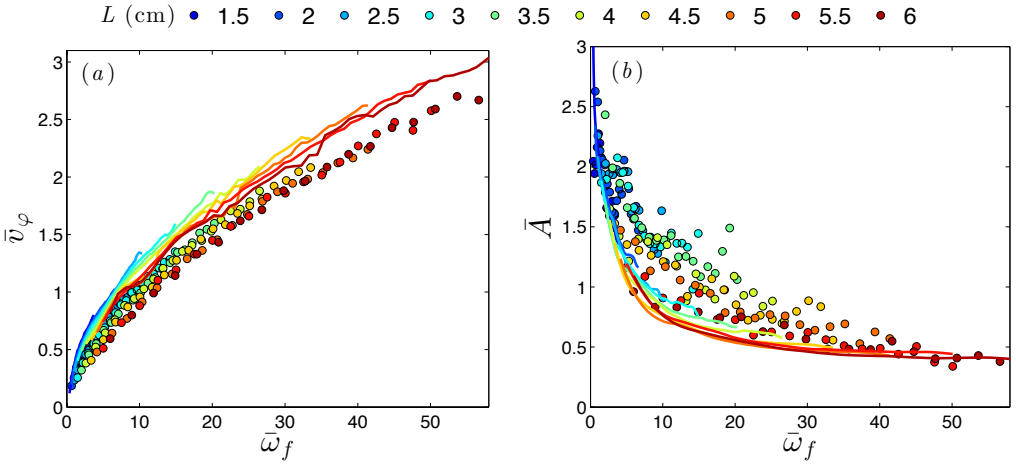

Figure 5.4: Comparison of experimental measurements (points) and output of the model (lines). (a) dimensionless phase velocity $\bar{v}_\varphi = v_\varphi/\omega_0 L$ and (b) Dimensionless amplitude of the oscillations $\bar{A} = A_r/A_f$. [Figures from 29]

amplitudes are involved, the non-linear inertial and curvature terms that appeared in Eq. 3.3 can here be neglected. The quadratic dissipation term opposing lateral motions is again present here and, remarkably, it turned out to be by large the most important effect of the fluid for the beam model, always one to two orders of magnitude larger than the added mass and flag terms [1]. The output of this model successfully recovered the elastic wave kinematics measured experimentally (see Fig. 5.4), and brought our attention to a crucial point: the irreversible loss of kinetic energy transferred from the swimmer body to the fluid (represented in the beam model by the quadratic dissipation term) is the dynamical ingredient that enables a propagative bending wave to be established. Indeed, removing this term completely changes the response of the system, where the bending wave no longer propagates but becomes a standing wave. We further analysed this problem in a simplified system with elastic strips vibrating in air and in water, which confirmed the previous observations (see [98]).

Now, back to Lighthill's model, considering a simplified kinematics $h(x,t) = A_r \cos(2\pi(ft - x/\lambda))$ characterised by the amplitude A_r and phase velocity $v_\varphi = f\lambda$ of the deformation wave recorded for the experimental swimmers (see Fig. 5.4), the estimate for the average propulsive force of Eq. 5.1 can be written as

$$\overline{T} = \frac{m}{4} A_r^2 \left(\frac{2\pi}{\lambda}\right)^2 \left[\, v_\varphi^2 - U^2 \,\right] , \tag{5.5}$$

while Eq. 5.3 for the efficiency becomes:

$$\eta = 1 - \frac{1}{2}\left(v_\varphi - U\right)/v_\varphi \, . \tag{5.6}$$

1. In the range of parameters of the experiment: $\tilde{m} \approx 1$, $\tilde{U} \approx [0.2 - 4]$ and $\tilde{\alpha} \approx [50 - 150]$. Eq. 5.4 is solved numerically using the experimental parameters (see [29]).

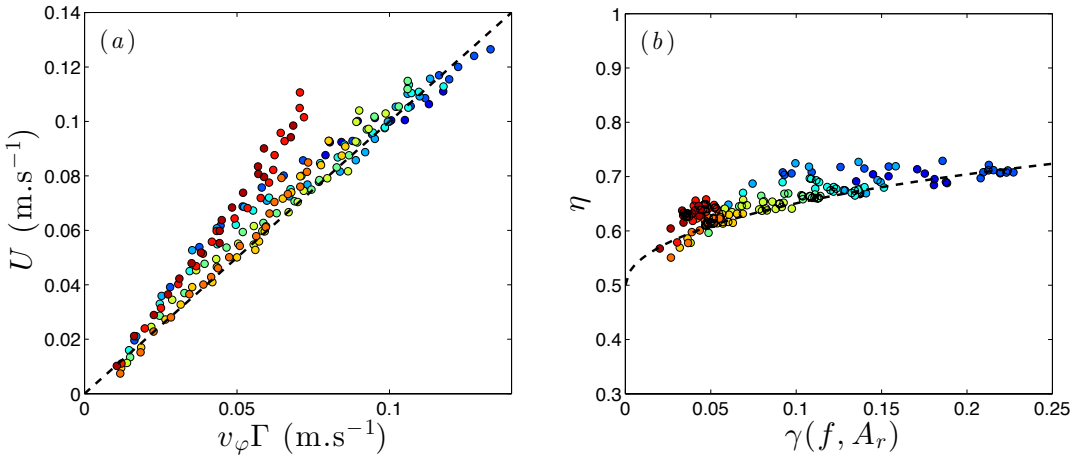

Figure 5.5: (*a*) Implementation of $U = \Gamma(\lambda, A_R; C_D)v_\varphi$ using experimental data. The line of slope unity around which the data lines up is the identity defined by Lighthill's theory. A single value of $C_D \approx 0.23$ was used, which is obtained as an adjustable parameter giving the best fit of all points. (*b*) Hydromechanical efficiency, calculated from Eq.5.6, plotted against γ which is a function of the kinematic characteristics of the swimmer. The dotted line corresponds to the $\eta(\gamma) = 1/2(1 + \sqrt{\gamma/(1+\gamma)})$ function issued from Lighthill's theory. [Figures from 29]

On the other hand, during cruising, the average thrust produced by a self-propelled swimmer is balanced by a mean drag force. We will discuss further this question in the next section. For the swimming filaments, we chose an equivalent bluff-body drag using the area swept by the tail of the swimmer as characteristic size, so that the average propulsive force is balanced by a mean global drag:

$$\overline{D} = \frac{1}{2}\rho U^2 C_D S', \tag{5.7}$$

where C_D is a drag coefficient and $S' = 2A_r \times d$ the effective section. Writing $\overline{T} = \overline{D}$ using Eqs. 5.5 and 5.7 we get an expression for the swimming speed in terms of the kinematic parameters of the swimmer $U = \Gamma(\lambda, A_R; C_D)v_\varphi$ —see Fig. 5.5 (a)—, where C_D serves as an adjusting parameter. The equation for the efficiency can now also be written in terms of the kinematics as $\eta = \frac{1}{2}(1 + \sqrt{\gamma/(1+\gamma)})$ with $\gamma = \gamma(\lambda, A_r; C_D)$ [see details in 29]. Figure 5.5 (b) shows the efficiency calculated directly from Eq. 5.6 using the experimental values for v_φ and U, as a function of γ, together with the theoretical prediction $\eta(\gamma)$, which gives a good representation of the experimental points. It can be seen that the efficiency increases with γ, giving in the present experiment values systematically higher than 1/2, which was shown by Lighthill [102] to be the maximum efficiency attainable by swimmers using standing waves as body undulations. To get a clearer view in terms of the body undulation kinematics we can write an approximate expression for $\lambda(f)$ using the dispersion relation of a beam submerged in quiescent fluid, which shows that $\gamma \propto A_r f$ [29]. The tendency in Fig. 5.5 (b) is thus that η increases with frequency, in spite of the diminishing flapping amplitude at the tail that accompanies an increasing frequency

in the present setup —see Fig. 5.4 (b)—.

The energy loss along the swimmer (represented in the beam model by the quadratic dissipation term) brings therefore an increase in efficiency, by determining the propagative dynamics to be established. Of course the same mechanism that enables the propagative dynamics by giving energy to the fluid, diminishes the amplitude of the oscillation. An interplay that will have to be considered in any design of flexible swimmers with localised actuation that use the elastic properties of the body to establish the undulation kinematics [2].

5.3 Self-propelled swimming foils

As we have mentioned, during cruising, the average thrust produced by a self-propelled swimmer is balanced by a global drag force. For a given object shape, this drag can involve skin friction or form drag, both being well-documented mechanisms. However, for swimmers whose shape is changing in time, the question of drag is not yet clearly established [see e.g. 109–111]. In the experiment described in the previous section with the free-surface swimmers, a form drag model using the area swept by the tail as characteristic size was assumed to balance the average thrust calculated using Lighthill's elongated-body theory and permitted to describe the observations [29]. Other experiments have used a skin friction model to complete a potential flow description of undulatory self-propelled swimmers [27].

We designed another experiment to address this problem, one that uses undulating thin flexible foils fully-submerged in a water tank, actuated by a pitching oscillation at one extremity to achieve self-propelled swimming (see Fig 5.6). Measurements of the propulsive performance together with full recording of the elastic wave kinematics were used to discuss the question of drag for different aspect ratio swimmers. The results showed, remarkably, that neither skin friction, nor form drag as used in the previous section, which both give expressions for drag per-unit-span, could explain the observed behaviour of the thrust coefficient C_T (see Fig. 5.7).

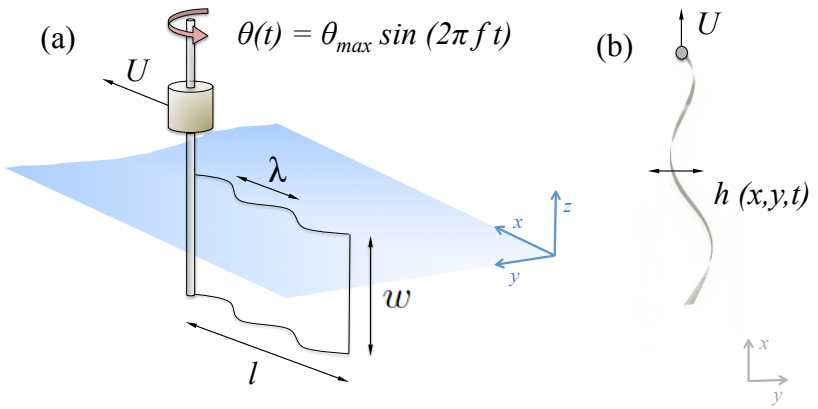

Figure 5.6: Experimental setup. (a) Sketch of the mechanical swimmer submerged in the tank. Definition of driving parameters as well as swimmer's dimensions and velocity. (b) Camera view of the swimmer. The local body deflection $h(x,y,t)$ is also indicated [Figure from 99].

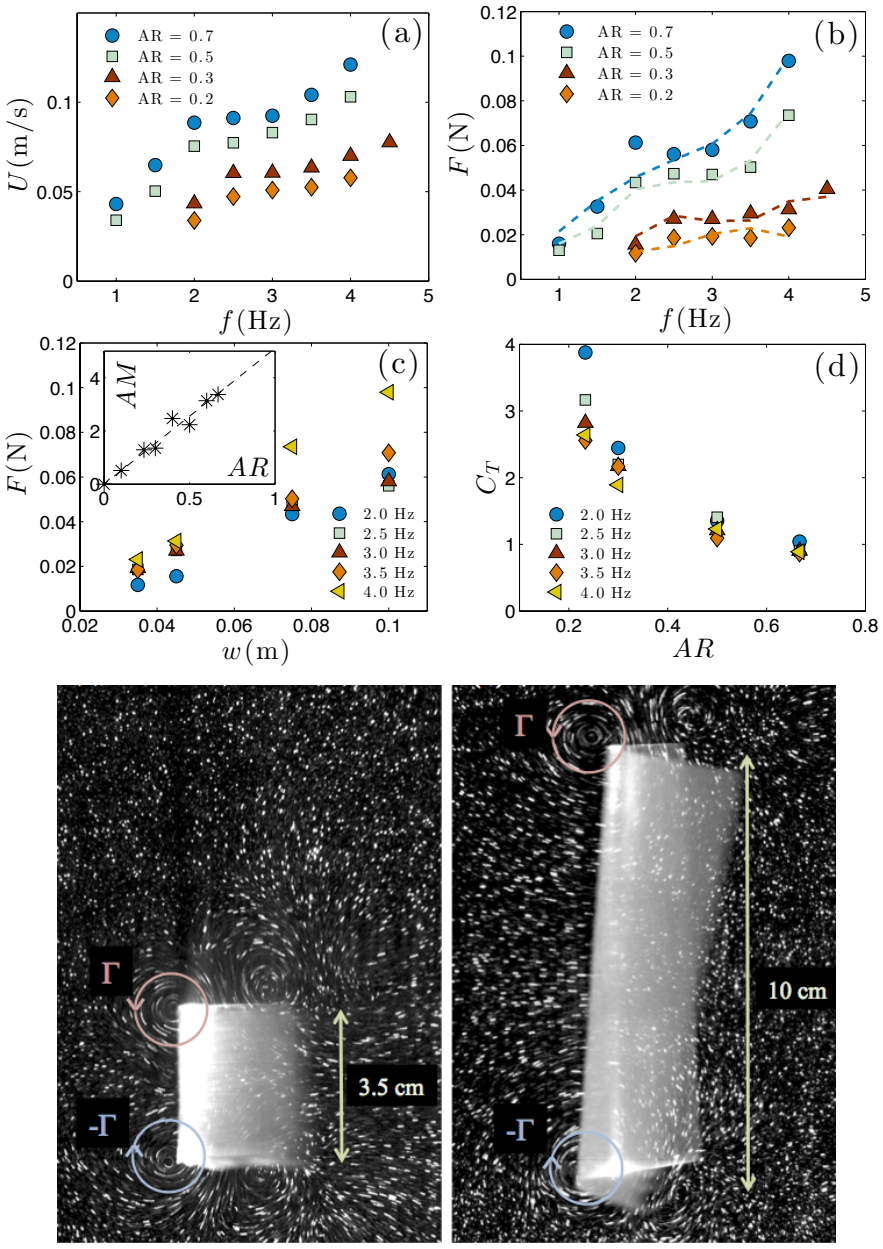

Figure 5.7: Top rows: (a) Self-propelled swimming velocity U as a function of the forcing frequency f for four aspect ratios. (b) and (c) Propulsive force F as a function of the forcing frequency and of the foil width, respectively. In (b) measurements are presented in symbols for different swimmers, together with the corresponding Lighthill's prediction using Eq. 5.1 (dashed lines), which allowed to calculate the added mass coefficient AM for each data set. The inset in (c) shows the added mass coefficient AM as a function of the aspect ratio AR. (d) Dimensionless thrust coefficient as a function of the aspect ratio. Bottom row: visualisation and schematic representation of the streamwise vortices rolling up at the lateral edges of two foils of different spans. [Figures from 99].

This prompted our attention to analysing the system considering finite size effects. We showed that a major part of the total drag comes from the trailing longitudinal vortices that roll-up on the lateral edges of the foils (see Fig. 5.7, bottom). This result gives a comparative advantage to swimming foils of larger span thus bringing new insight to the role of aspect ratio for undulatory swimmers (see [99]).

6. Perspectives

Rather than closing this review with a summary of the results and conclusions mentioned in the previous chapters, let us attempt a brief account of the research lines that we can foresee for the future (some of which are by now already being pursued). A few sections follow, grouped in subjects that sometimes appear too rigid, when the questions we ask overlap among more than one theme, revealing of course the richness of these subjects.

6.1 Insect flight

Our future goal concerning flapping flyers is to get a bit closer to the engineering perspective of the problem of insect flight. We would like to ask which are the fundamental points, beyond the well studied aerodynamical aspects, to be understood if we want to consider building insect-inspired flying robots that are both versatile and energy efficient?

Although bio-inspiration is not a new concept in the search for innovative solutions to engineering problems, in the case of flapping-wing flyers a review of the literature tells us that most research efforts have been concentrated in the aerodynamic questions. Wing aerodynamics is certainly a major player in this problem, as shown in the problems discussed in Chapter 3, but recent studies also point out that the outcome of wing motion, in terms of production of useful propulsive or manoeuvring forces, is intimately linked to the dynamics of other parts of the body such as the thorax, abdomen and legs (e.g. the initial leg force in the take-off of the butterflies of Chapter 4). This observation constitutes the seed for one of the main objectives we attempt to follow in the future, which is to go beyond the sole aerodynamics of flapping wings, a subject where a large amount of studies is now available [84], and to consider different aspects of the relevant multi-body dynamics. To this end, we propose to pursue a cross-disciplinary program involving experimental biology tasks with a few insect species, as well as physics and mechanics modelling using experimental and theoretical tools [see e.g. 113]. In addition to further work concerning the take-off maneuver with the white cabbage pierid described in chapter 4, we have identified the common green lacewing *Chrysopa carnea* as suitable model to study forewing-hindwing interactions with very flexible wings, and the spider wasp (pompilidae) as an extreme model to investigate multi-body dynamics (see Figure 6.1). Studying the biomechanics of the whole insect will let us ponder the role of the diverse mechanisms that govern performance and efficiency in flapping flyers.

Biologically-inspired flying robots are by now the object of several engineering programs because of a vast set of useful applications. Among other things, one may think of military or civil surveillance missions, or maintenance and remediation tasks in environmentally compromised sites. Well-controlled small-scale flapping wing vehicles are by now starting to become a reality

Figure 6.1: (a) *Pieris rapae*, (b) *Chrysopa carnea*, (c) Pompilidae wasp [Photos from 112].

(see e.g. [114]). However, long-duration power autonomy is still not, and these insect-scale robots are still tethered to their power chord. How can we increase flight duration and optimise manoeuvrability? One path to try to solve this problem is of course to pursue research in the area of small, high-energy-density power sources, which is certainly being done elsewhere (e.g. [115]). That approach consists in increasing energy availability. Our future efforts will explore the other, symmetric path: the one that has to do with the way biomechanics, i.e. kinematics of body parts and material properties, minimise energy consumption. Here the core questions are to be identified in the relation between body kinematics, performance and energy expenditure [1].

6.2 Smaller swimmers and micro-swimmers

Our work with magnetically-actuated small swimmers described in Chapter 5 has brought a series of perspectives that we have already started exploring. An interesting path comes from decreasing the size of the problem, which triggers the question of inertial-to-viscous regime transition for undulatory swimmers. From the biological standpoint, such a regime transition is for example associated to the process of development, where the locomotion of young fish or larvae is subjected to dynamical constraints mostly ruled by viscosity, but which will progressively incorporate inertial effects as their body increases in size (see Fig. 6.2 and Ref. [116]). This is one of the subjects we are currently working on, where diminishing the size of our surface swimmers raises other complex questions such as the increasing role of the capillary effects. In the study described in chapter 5, surface tension was considered only implicitly as an experimental means of keeping the model two-dimensional by making the swimmer move on the air-water interface. For smaller swimmers, however, the relative size of the meniscus will most likely perturb this simplistic view and call for a new description, where other interesting problems such as the effect of the surface roughness of the swimmer skin can be included. One may think of the dynamical role of superhydrophobicity, which has been pointed out as an important matter

1. This project is the subject of an ongoing collaboration with Jérôme Casas (IRBI, Tours).

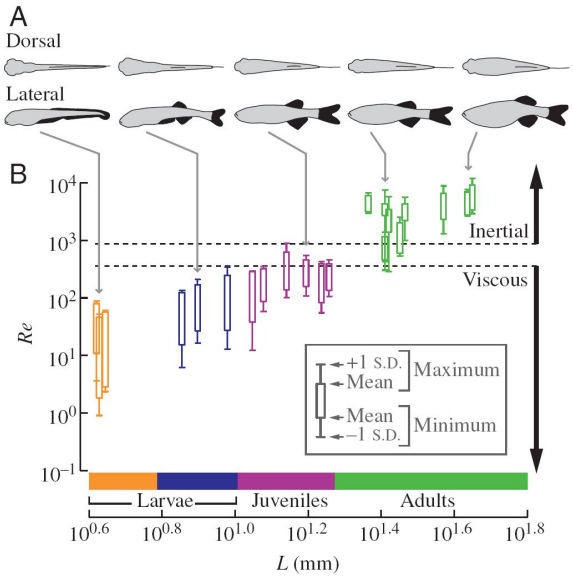

Figure 6.2: Reynolds numbers spanned during coasting by zebrafish of different size (Figure reproduced from McHenry & Lauder, 2005 [116]).

in some cases such as the locomotion of water-walking arthropods, not only for its well-studied water-repellency properties but also as a drag reduction mechanism [117].

Forgetting the free surface effects, the subject can also get richer when considering the interaction between many swimmers. This is another goal of our current research, which we are pursuing in the context of newly developed micro-swimmers. Different sorts of magnetic materials such as aggregates of micron-sized super-paramagnetic particles [118] are being tested (see Fig. 6.3) and, undoubtedly, the Reynolds number is shrinking [1].

Biomedical applications abound for artificial micro-swimmers, which go from performing missions of targeted drug delivery to microsurgery. Wireless micro-robots offer indeed great promises in the development of minimally invasive medical procedures [119]. The idea of a swarm of actively-controlled swimmers being able to self-propel and perform a task inside the human body is certainly appealing, and clever solutions in the form of active control by magnetic fields have been offered [120], where the design of the artificial swimmers uses an external magnetic field to induce motion. An external magnetic field creates a convenient solution to the problem of supplying power to the swimmer. Not only does externalising the power supply lend itself to easier scale-down in size, but also, the magnetic field can be incorporated into a magnetic resonance scanner, or MRI, a tool already commonplace in hospitals, to combine actuation and imaging in one [121]. However, many questions still remain open, especially concerning the interaction of an artificial swimmer with its environment and the collective dynamics inherent to a group of swimmers. The latter is a flourishing field of current research known as

1. This project has been developed by Miguel Piñeirua (postdoctoral fellow 2014-2015, co-advised with Benjamin Thiria).

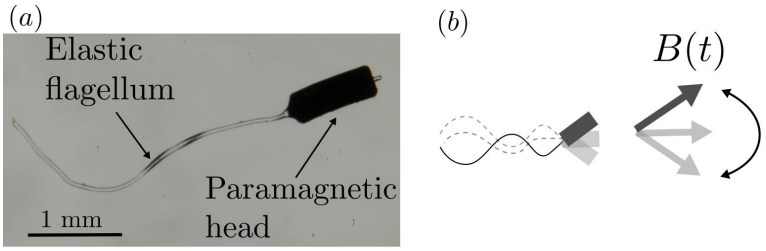

Figure 6.3: (a) Example of experimental flagellated PDMS micro-swimmers currently being tested. (b) Schematic diagram of the magnetic field $B(t)$ used to drive the oscillation of a paramagnetic head. (Photo and diagram by M. Piñeirua).

active matter [see e.g. 122], which is defined as a fluid constituted by large numbers of active, self-propelled entities that give rise to collective effects modifying the effective properties of the solution. Anomalous properties of active suspensions include, for instance, the enhanced diffusion of chemicals or other passive entities due to the presence of swimming bacteria [123], or the collective clustering of swimmers into biofilms [124]. These unique hydrodynamic properties of active suspensions promise many exciting new applications, such as the use of artificial micro-swimmers as active transport agents in the human body. Biological organisms in their natural environment provide of course inspiration for the design of such artificial swimmers. The experimental backbone of our future research effort on this subject will be built upon a down-scaled version of the elastic swimmers of Chapter 5, containing a small magnetic head and a cylindrical elastic tail. We will consider swimmer-wall interactions [125; 126], swimmer-swimmer interactions, and many-body collective dynamics, all being fundamental issues concerning the perspective of using artificial swimmers for the targeted delivery purposes mentioned above. Additionally, while biological organisms serve as inspiration for the design of artificial swimmers [127–130], artificial swimmers in return can lend themselves to a deeper understanding of the biological organisms they mimic and thus can be used to address biologically-relevant issues; for instance, in the public health domain, sperm swimming speed is significantly related to fertilization success [131].

6.3 Undulatory swimming

We have evoked collective and boundary effects in the previous section thinking about micro-swimmers. But these questions about interactions arise of course also in the larger scales that we have discussed in chapter 5. Moreover, they are crucial for the understanding of real systems. For example, batoids and flatfish generally swim very close to the substrate, whereas most aquatic mammals can spend long periods of time swimming just below the sea surface. Despite the successes of Lighthill's theory, the ubiquitous problems of the interaction between a swimmer and a wall or a free surface are out of its reach. This is also the case for the description of the interactions between multiple swimmers, which may significantly impact the performance or cost of locomotion associated with fish schooling, as each swimmer moves in a non-uniform

Figure 6.4: Two self-propelled swimmers in a side-by-side configuration. Each foil is held by an independent air-bearing rail. In the image sequence presented the two foils are actuated in anti-phase.

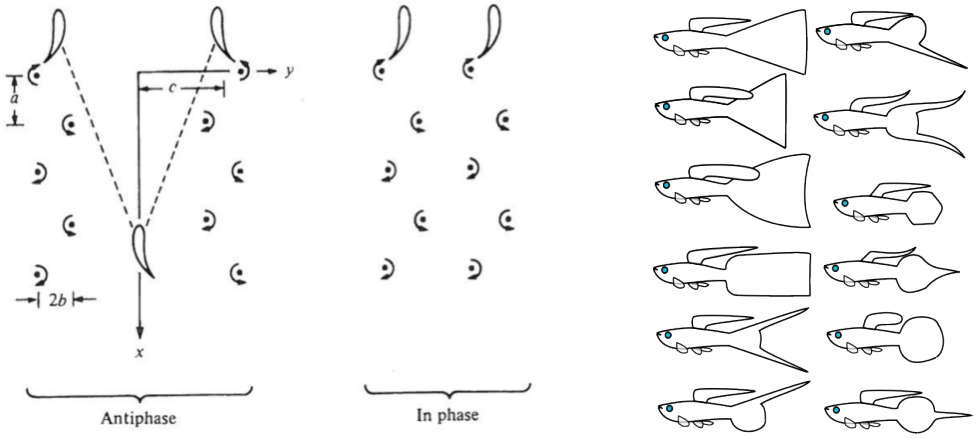

Figure 6.5: Left: Theoretical vortex wakes for interacting swimmers [From Childress, 1981, 31]. Right: Standard tails for guppies *(Poecilia reticulata)*. [From Wikimedia Commons]

and unsteady flow created by its neighbours. We have already used the experiment described in Chapter 5 on a swimming foil to study the effect of swimming near a wall, establishing the main physical mechanism, a reorientation of momentum, that leads to a performance enhancement due to the presence of the wall [100]. The full fluid-structure interaction problem linking the large amplitude passive deformation of our flexible swimmer to the constraints imposed by the boundary remains to be addressed, as is the extension of the study to the case of swimming near a free-surface which is a deformable boundary.

Ongoing work concerns an extension of the previous experiment with the swimming foils to explore hydrodynamic swimmer-swimmer interactions [1]. We concentrate at present on the simplest situation with only two swimmers (see Fig. 6.4), in order to be able to quantify accurately the interaction processes. We expect in this way to provide a valuable input for the modelling of collective effects in systems with a large number of swimmers, where one-on-one interactions constitute the building blocks (see e.g. the classic picture in Fig. 6.5, left). An additional

1. This is part of the PhD project of Intesaaf Ashraf (2014-2017, co-advised with Benjamin Thiria).

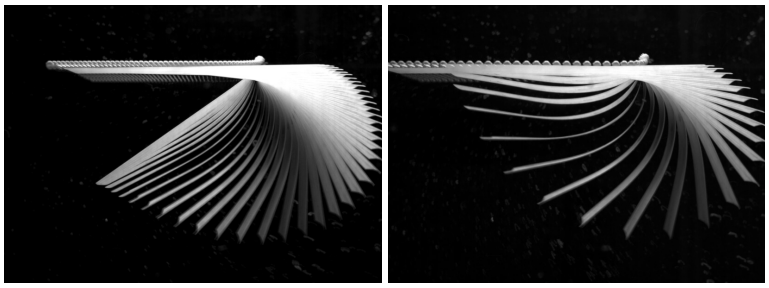

Figure 6.6: Start-up motion of a flexible sheet from two different initial angles. The escape direction is from right to left, following a counterclockwise rotation of the foil shown here by superposed snapshots separated by a $\Delta T = 0.1$s time lapse. (Photos by R. Zenit, publication in preparation [132]).

experimental project concerning the collective dynamics of swimmers with flexible propulsors is the use of a real biological model. The idea comes from the observation of small aquarium fish with very flexible caudal fins where a deformation wave actuated at the peduncle of the tail is propagated passively, much like the flexible foils of our experiments in Chapter 5. Different kinds of guppies (see Fig. 6.5, right) seem like an ideal model, and we are currently designing a swimming channel connected to an aquarium that will allow us to examine swimmer-swimmer interactions in real swimmers but in a controlled situation. This project brings the additional technical challenge for our fluid dynamics laboratory of learning the proper experimental protocols to work with live fish, especially if we consider performing PIV measurements.

6.4 Transient regimes

In most of the swimming and flying examples that we have discussed we have considered the *cruising* regime, i.e. we have analysed the effect of variations in different geometrical and/or actuation parameters on the observed average velocity of locomotion. The exception in the previous pages is the study of the take-off flight of the pierid butterfly, where we have focused on a transient maneuver. For the case of insects, as we have seen, this take-off maneuver involves not only aerodynamics but the mechanics of the full insect. We have already noted above that this multi-body dynamics will be a crucial point of our future work.

But transient maneuvers are everywhere and in the context of bio-inspired swimming and flying they have been much less studied than cruising regimes. Using our flexible foil models we have already started considering a minimal model of the C-start maneuver [1], the archetype of fish fast-start swimming which involves an initial phase where the animal bends its body into a C-shape before producing a powerful recovery stroke that drives its sudden acceleration. Using the setup of Chapter 5, described in Fig. 5.6, we produced a synthetic C-start maneuver by operating an impulsive rotational actuation on one extremity of the foil. The deformation kinematics being governed by the foil flexibility, as the foil rotates, it pushes the surrounding fluid, it deforms passively and stores elastic energy. The latter will drive the recovery of the

1. In collaboration with Roberto Zenit from UNAM, México

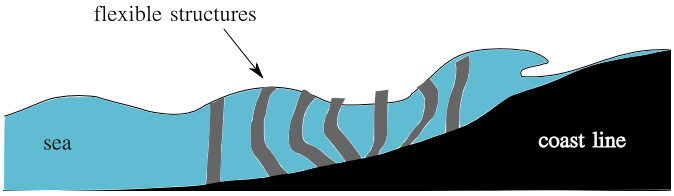

Figure 6.7: Schematic diagram of a possible configuration of flexible rods subjected to the action of a surface wave field.

straight body shape after the motor actuation has stopped as shown in Fig. 6.6. During the rotation of the foil a thrust force is induced, which drives the synthetic escape maneuver. We measure the resulting escape velocity and acceleration as a function of the geometric parameters of the foil and of the imposed forcing.

Another starting project where the important questions intrinsically concern transient regimes is the study of the aquatic snake strike, a project in collaboration with the Muséum National d'Histoire Naturelle [1]. From the biological point of view, the hydrodynamic constrains are expected to be a fundamental element in the morphological convergence of the head shapes observed in different aquatic snake species [133]. The questions on drag and added mass that we have discussed in Chapter 5 will have to be reformulated to establish the different balances that can be expected when comparing the transient attack maneuver and other swimming regimes.

6.5 Energy transfers in fluid-elasticity problems

An opening that has emanated from our reflection on fluid-structure interaction problems goes beyond bio-locomotion and into the domain of energy transfers and renewable energies. Formally the problems are similar, the main difference being that in the locomotion problem the propulsive appendage is actuated to produce a force, whereas in the energy absorption problem the net energy transfer is reversed. Recent research abounds on different energy-harvesting devices using elastic structures [see e.g. 134–136], and the useful analytic tools in such problems join those that we have used for the locomotion problems. A particularly interesting case, just like in the case of undulatory swimming, concerns the collective effects of multiple structures interacting. In this perspective, we are starting a project concerning the interaction of elastic structures with surface waves (see Fig. 6.7), as a proof of concept for an energy absorbing system with potential applications in coastline protection and energy harvesting. The idea is that an array of elastic slender structures (e.g. cylindrical rods) can be installed along the shore, where wave-energy absorption can be tuned by controlling the transformation of flow kinetic energy into potential energy in the elastic deformation. The later can in turn be either dissipated or electrically harvested. Such systems could become integral costal management tools, acting as artificial underwater canopies with other potential parallel applications such as controlling transport of pollutants [137].

1. Marion Segall's PhD project (2014-2017, co-advised with Anthony Herrel, CNRS/MNHN).

References

[1] C. MARAIS. *Dynamique tourbillonnaire dans le sillage d'un aileron oscillant : Propulsion par ailes battantes biomimétiques*. PhD thesis, Université Paris Diderot, 2011. vii

[2] S. RAMANANARIVO. *Propulsion biomimétique de structures élastiques*. PhD thesis, Université Paris Diderot, 2014. vii, 45, 49

[3] C. MARAIS, R. GODOY-DIANA, D. BARKLEY, AND J. E. WESFREID. **Convective instability in inhomogeneous media: Impulse response in the subcritical cylinder wake**. *Phys. Fluids*, **23**(1):014104, 2011. viii

[4] J. D'ADAMO, R. GODOY-DIANA, AND J. E. WESFREID. **Spatiotemporal spectral analysis of a forced cylinder wake**. *Phys. Rev. E*, **84**(5):056308, 2011. viii

[5] J. D'ADAMO, R. GODOY-DIANA, AND J. E. WESFREID. **Centrifugal instability of Stokes layers in crossflow: the case of a forced cylinder wake**. 2014. Submitted. viii

[6] R. GODOY-DIANA AND S. P. R. CZITROM. **On the tuning of a wave-energy driven oscillating-water-column seawater pump to polychromatic waves**. *Ocean Eng.*, **34**(17-18):2374–2384, 2007. viii

[7] G. R. SPEDDING. **The aerodynamics of flight**. In R. M. ALEXANDER, editor, *Mechanics of Animal Locomotion*, **11** of *Advances in Comparative and Environmental Physiology*, pages 52–111. Springer-Verlag, 1992. 12

[8] S. P. SANE. **The aerodynamics of insect flight**. *J. Exp. Biol.*, **206**(23):4191–4208, 2003. 12

[9] D. E. ALEXANDER. *Nature's flyers: birds, insects, and the biomechanics of flight*. JHU Press, 2004. 12

[10] R. MACARTHUR AND R. LEVINS. **The limiting similarity, convergence, and divergence of coexisting species**. *Am. Nat.*, pages 377–385, 1967. 12

[11] G. J. ROMANES. *Darwin and after Darwin: An exposition of the Darwinian theory and a discussion of post-Darwinian questions*. The Open Court Publishing Company, 1892. 12

[12] R. J. WOOTTON. **Functional morphology of insect wings**. *Annu. Rev. Entomol.*, **37**(1):113–140, 1992. 12

[13] S. A. COMBES AND T. L. DANIEL. **Flexural stiffness in insect wings I. Scaling and the influence of wing venation**. *J. Exp. Biol.*, **206**(17):2979, 2003. 13, 30

[14] A. M. MOUNTCASTLE AND T. L. DANIEL. **Aerodynamic and functional consequences of wing compliance**. *Exp. Fluids*, **46**(5):873–882, May 2009. 13

[15] G. B. GILLIS. **Undulatory Locomotion in Elongate Aquatic Vertebrates: Anguilliform Swimming since Sir James Gray**. *American Zoologist*, **36**(6):656–665, 1996. 13

[16] E. LAUGA AND T. POWERS. **The hydrodynamics of swimming microorganisms**. *Reports on Progress in Physics*, **72**:096601, 2009. 13

[17] T. Y. WU. **Fish Swimming and Bird/Insect Flight**. *Annu. Rev. Fluid Mech.*, **43**(1):25–58, January 2011. 13, 44

[18] J. J. VIDELER. *Fish swimming*, **10**. Springer, 1993. 13

[19] R. W. BLAKE. **Fish functional design and swimming performance**. *J. Fish Biol.*, **65**(5):1193–1222, November 2004. 13

[20] M. SFAKIOTAKIS, D. M. LANE, AND J. B. C. DAVIES. **Review of fish swimming modes for aquatic locomotion**. *IEEE J. Ocean. Eng.*, **24**(2):237–252, 1999. 13

[21] M. S. TRIANTAFYLLOU, G. S. TRIANTAFYLLOU, AND D. K. P. YUE. **Hydrodynamics of Fishlike Swimming**. *Annu. Rev. Fluid Mech.*, **32**(1):33–53, 2000. 13, 15

[22] P. W. WEBB. **Body Form, Locomotion and Foraging in Aquatic Vertebrates**. *Am. Zool.*, **24**(1):107–120, 1984. 13

[23] P. W. WEBB. **The biology of fish swimming**. In L. MADDOCK, Q. BONE, AND J. M. V. RAYNER, editors, *Mechanics and Physiology of Animal Swimming*, pages 45–62. Cambridge University Press, 1994. 13, 14

[24] T. J. PEDLEY AND S. J. HILL. **Large-amplitude undulatory fish swimming: fluid mechanics coupled to internal mechanics**. *J. Exp. Biol.*, **202**(23):3431, 1999. 13

[25] A. CRESPI, A. BADERTSCHER, A. GUIGNARD, AND A. J. IJSPEERT. **AmphiBot I: an amphibious snake-like robot**. *Robotics and Autonomous Systems*, **50**(4):163–175, March 2005. 13

[26] MS TRIANTAFYLLOU AND GS TRIANTAFYLLOU. **An efficient swimming machine**. *Scientific American*, **272**(3):64–71, 1995. 13

[27] S ALBEN, C WITT, TV BAKER, E ANDERSON, AND G LAUDER. **Dynamics of freely swimming flexible foils**. *Phys. Fluids*, **24**:051901, 2012. 14, 49

[28] P A DEWEY, B M BOSCHITSCH, K W MOORED, H A STONE, AND A J SMITS. **Scaling laws for the thrust production of flexible pitching panels**. *J. Fluid Mech.*, **732**:29–46, 2013.

[29] S RAMANANARIVO, R GODOY-DIANA, AND B THIRIA. **Passive elastic mechanism to mimic fish-muscle action in anguilliform swimming**. *J. Roy. Soc. Interface*, **10**(88):20130667–20130667, 2013. 14, 43, 46, 47, 48, 49

[30] E. GUYON, J. P. HULIN, AND L. PETIT. *Hydrodynamique physique*. EDP sciences / CNRS Éditions, 3e edition edition, 2012. 15

[31] S. CHILDRESS. *Mechanics of swimming and flying*. Cambridge Studies in Mathematical Biology, 1981. 15, 44, 57

[32] S. MICHELIN, S. G. LLEWELLYN SMITH, AND B. J. GLOVER. **Vortex shedding model of a flapping flag**. *J. Fluid Mech.*, **617**(1), 2008. 15

[33] S. ALBEN. **Simulating the dynamics of flexible bodies and vortex sheets**. *J. Comp. Phys.*, **228**(7):2587–2603, 2009.

[34] J. X. SHENG, A. YSASI, D. KOLOMENSKIY, E. KANSO, M. NITSCHE, AND K. SCHNEIDER. **Simulating Vortex Wakes of Flapping Plates**. In S. CHILDRESS, A. HOSOI, W. W. SCHULTZ, AND Z. J. WANG, editors, *Natural Locomotion in Fluids and on Surfaces*, pages 255–262. Springer, 2012. 15

[35] K. V. ROZHDESTVENSKY AND V. A. RYZHOV. **Aerohydrodynamics of flapping-wing propulsors**. *Progr. Aerospace Sci.*, **39**:585–633, 2003. 15

[36] M. S. TRIANTAFYLLOU, A. H. TECHET, AND F. S. HOVER. **Review of experimental work in biomimetic foils**. *IEEE J. Ocean. Eng.*, **29**(3):585–594, 2004.

[37] Z. J. WANG. **Dissecting insect flight**. *Annu. Rev. Fluid Mech.*, **37**:183–210, 2005.

[38] F. E. FISH AND G. V. LAUDER. **Passive and Active Flow Control by Swimming Fishes and Mammals**. *Annu. Rev. Fluid Mech.*, **38**:193–224, 2006. 15

[39] O. DOARÉ. *Interaction fluide-strucutre (Cours MS-206)*. ENSTA ParisTech, 2010. 16

[40] M. P. PAIDOUSSIS. *Fluid-Structure Interactions: Slender Structures and Axial Flow*. Number v. 1 in Fluid-structure Interactions: Slender Structures and Axial Flow. Elsevier Science, 1998. 17

[41] R. GODOY-DIANA, C. MARAIS, J. L. AIDER, AND J. E. WESFREID. **A model for the symmetry breaking of the reverse Benard-von Karman vortex street produced by a flapping foil**. *J. Fluid Mech.*, **622**:23–32, 2009. 19, 21, 22

[42] R GODOY-DIANA, J L AIDER, AND J E WESFREID. **Transitions in the wake of a flapping foil**. *Phys. Rev. E*, **77**(1):016308, 2008. 19, 21, 24

[43] C MARAIS, B THIRIA, J E WESFREID, AND R GODOY-DIANA. **Stabilizing effect of flexibility in the wake of a flapping foil**. *J. Fluid Mech.*, **710**:659–669, September 2012. 19, 23, 25

[44] V RASPA, R GODOY-DIANA, AND B THIRIA. **Topology-induced effect in biomimetic propulsive wakes**. *J. Fluid Mech.*, **729**:377–387, 2013. 19, 25, 26, 27

[45] M. J. WOLFGANG, J. M. ANDERSON, M. A. GROSENBAUGH, D. K. P. YUE, AND M. S. TRIANTAFYLLOU. **Near-body flow dynamics in swimming fish**. *J. Exp. Biol.*, **202**:2302–2327, 1999. 20

[46] E. G. DRUCKER AND G. V. LAUDER. **Locomotor function of the dorsal fin in teleost fishes: experimental analysis of wake forces in sunfish**. *J. Exp. Biol.*, **204**:2943–2958, 2001. 20

[47] M. M. KOOCHESFAHANI. **Vortical patterns in the wake of an oscillating airfoil**. *AIAA J.*, **27**(9):1200–1205, 1989. 20

[48] R. GOPALKRISHNAN, M. S. TRIANTAFYLLOU, G. S. TRIANTAFYLLOU, AND D. BARRETT. **Active vorticity control in a shear flow using a flapping foil**. *J. Fluid Mech.*, **274**:1–21, 1994.

[49] J. M. ANDERSON, K. STREITLIEN, D. S. BARRET, AND M. S. TRIANTAFYLLOU. **Oscillating foils of high propulsive efficiency**. *J. Fluid Mech.*, **360**:41–72, 1998. 20

[50] K. D. JONES, C. M. DOHRING, AND M. F. PLATZER. **Experimental and computational investigation of the Knoller-Betz effect**. *AIAA J.*, **36**(7):1240–1246, 1998. 20

[51] J. C. S. LAI AND M. F. PLATZER. **Jet characteristics of a plunging airfoil**. *AIAA J.*, **37**(12):1529–1537, 1999.

[52] N. VANDENBERGHE, J. ZHANG, AND S. CHILDRESS. **Symmetry breaking leads to forward flapping flight**. *J. Fluid Mech.*, **506**:147–155, 2004.

[53] K. PARKER, K. D. VON ELLENRIEDER, AND J. SORIA. **Using stereo multigrid DPIV (SMDPIV) measurements to investigate the vortical skeleton behind a finite-span flapping wing**. *Exp. Fluids*, **39**:281–298, 2005.

[54] J. H. J. BUCHHOLZ AND A. J. SMITS. **On the evolution of the wake structure produced by a low-aspect-ratio pitching panel**. *J. Fluid Mech.*, **546**:433–443, 2006. 20, 21

[55] Q. ZHU, M. J. WOLFGANG, D. K. P. YUE, AND M. S. TRIANTAFYLLOU. **Three-dimensional flow structures and vorticity control in fish-like swimming**. *J. Fluid Mech.*, **468**:1–28, 2002. 20

[56] L. GUGLIELMINI, P. BLONDEAUX, AND G. VITTORI. **A simple model of propulsive oscillating foils**. *Ocean Eng.*, **31**(7):883–899, 2004.

[57] S. ALBEN AND M. SHELLEY. **Coherent locomotion as an attracting state for a free flapping body**. *Proc. National Ac. Sci. (USA)*, **102**(32):11163–11166, 2005.

[58] P. BLONDEAUX, F. FORNARELLI, L. GUGLIELMINI, M. S. TRIANTAFYLLOU, AND R. VERZICCO. **Numerical experiments on flapping foils mimicking fish-like locomotion**. *Phys. Fluids*, **17**:113601, 2005.

[59] H. DONG, R. MITTAL, AND F. M. NAJJAR. **Wake topology and hydrodynamic performance of low-aspect-ratio flapping foils**. *J. Fluid Mech.*, **566**:309–343, 2006. 20

[60] G. K. TAYLOR, R. L. NUDDS, AND A. L. R. THOMAS. **Flying and swimming animals cruise at a Strouhal number tuned for high power efficiency**. *Nature*, **425**:707–711, 2003. 20

[61] M. S. TRIANTAFYLLOU, G. S. TRIANTAFYLLOU, AND R. GOPALKRISHNAN. **Wake mechanics for thrust generation in oscillating foils**. *Phys. Fluids A*, **3**(12):2835–2837, 1991. 20

[62] K. D. VON ELLENRIEDER, K. PARKER, AND J. SORIA. **Flow structures behind a heaving and pitching finite-span wing**. *J. Fluid Mech.*, **490**:129–138, 2003. 21

[63] J. H. J. BUCHHOLZ AND A. J. SMITS. **The wake structure and thrust performance of a rigid low-aspect-ratio pitching panel**. *J. Fluid Mech.*, **603**:331–365, 2008. 21

[64] T SCHNIPPER, A ANDERSEN, AND T BOHR. **Vortex wakes of a flapping foil**. *J. Fluid Mech.*, **633**:411, 2009. 21

[65] G. Y. He, Q. Wang, X. Zhang, and S. G. Zhang. **Numerical analysis on transitions and symmetry-breaking in the wake of a flapping foil**. *Acta Mechanica Sinica*, **28**(6):1551–1556, December 2012.

[66] D. B. Quinn, G. V. Lauder, and A. J. Smits. **Scaling the propulsive performance of heaving flexible panels**. *J. Fluid Mech.*, **738**:250–267, 2014. 21

[67] B. Thiria, S. Goujon-Durand, and J. E. Wesfreid. **Wake of a cylinder performing rotary oscillations**. *J. Fluid Mech.*, **560**:123–147, 2006. 21

[68] D. J. Cleaver, Z. Wang, and I. Gursul. **Bifurcating flows of plunging aerofoils at high Strouhal numbers**. *J. Fluid Mech.*, **708**:349–376, August 2012. 22

[69] Z. C. Zheng and Z. Wei. **Study of mechanisms and factors that influence the formation of vortical wake of a heaving airfoil**. *Physics of Fluids (1994-present)*, **24**(10):103601, 2012.

[70] I. Gursul, D. J. Cleaver, and Z. Wang. **Control of low Reynolds number flows by means of fluidâĂŞstructure interactions**. *Progr. Aerospace Sci.*, **64**(0):17 – 55, 2014.

[71] Z. Wei and Z. C. Zheng. **Mechanisms of wake deflection angle change behind a heaving airfoil**. *J. Fluids Struct.*, **48**(0):1 – 13, 2014. 22

[72] S.B. Pope. *Turbulent flows*. Cambridge University Press, 2000. 27

[73] G. K. Batchelor. *An introduction to fluid dynamics*. Cambridge University Press, 1967. 27

[74] G.R. Spedding and A. Hedenström. **PIV-based investigations of animal flight**. *Exp. Fluids*, **46**(5):749–763, 2009. 27

[75] A. Magnan. *La locomotion chez les animaux: I-Le vol des insectes*. Hermann & Cie., 1934. 29

[76] B. Thiria and R. Godoy-Diana. **How wing compliance drives the efficiency of self-propelled flapping flyers**. *Phys. Rev. E*, **82**:015303(R), 2010. 29, 30, 31, 32

[77] S. Ramananarivo, R. Godoy-Diana, and B. Thiria. **Rather than resonance, flapping wing flyers may play on aerodynamics to improve performance**. *Proc. National Ac. Sci. (USA)*, **108**(15):5964–5969, 4 2011. 29, 32, 33, 34, 35

[78] R. Godoy-Diana, P. Jain, M. Centeno, A. Weinreb, and B. Thiria. **Forewing-hindwing phase-lag effect in the propulsive performance of a four-winged flapping flyer**. In J. Klapp, G. Ruíz, A. Medina, A. López, and L. G. Sigalotti, editors, *Selected Topics of Computational and Experimental Fluid Mechanics*, Environmental Science and Engineering. Springer, 2015. In press. 29, 37

[79] T. L. Daniel and S. A. Combes. **Flexible wings and fins: Bending by inertial or fluid-dynamic forces?** *Integrative and Comparative Biology*, **42**(5):1044, 2002. 31

[80] J. Bico, B. Roman, L. Moulin, and A. Boudaoud. **Elastocapillary coalescence in wet hair**. *Nature*, **432**(7018):690–690, dec 2004. 31

[81] S Alben, M Shelley, and J Zhang. **Drag reduction through self-similar bending of a flexible body**. *Nature*, **420**(6915):479–481, 2002. 31

[82] L Schouveiler and A Boudaoud. **The rolling up of sheets in a steady flow**. *J. Fluid Mech.*, **563**:71–80, 2006.

[83] F Gosselin, E de Langre, and BA Machado-Almeida. **Drag reduction of flexible plates by reconfiguration**. *J. Fluid Mech.*, **650**:319–341, 2010. 31

[84] W. Shyy, H. Aono, S. K. Chimakurthi, P. Trizila, C. K. Kang, C. E .S. Cesnik, and H. Liu. **Recent progress in flapping wing aerodynamics and aeroelasticity**. *Progr. Aerospace Sci.*, **46**(7):284–327, 2010. 34, 53

[85] S. E. Spagnolie, L. Moret, M. J. Shelley, and J. Zhang. **Surprising behaviors in flapping locomotion with passive pitching**. *Phys. Fluids*, **22**(4):041903, 2010. 34

[86] J. Zhang, L. Nan-Sheng, and L. Xi-Yun. **Locomotion of a passively flapping flat plate.** *J. Fluid Mech.* **In press.** *J. Fluid Mech.*, **659**:43–68, 2010. 34

[87] H. MASOUD AND A. ALEXEEV. **Resonance of flexible flapping wings at low Reynolds number**. *Phys. Rev. E*, **81**(5):056304, May 2010. 34

[88] C P ELLINGTON. **The Aerodynamics of Hovering Insect Flight. I. The quasisteady analisys. II. Morphological paramters. III. Kinematics. IV. Aerodynamic mechanisms. V. A vortex theory. VI. Lift and power requirements**. *Phil. Trans. Roy. Soc. B*, **305**(1122):1–181, February 1984. 35

[89] D. LENTINK AND M. H. DICKINSON. **Biofluiddynamic scaling of flapping, spinning and translating fins and wings**. *J. Exp. Biol.*, **212**(16):2691–2704, August 2009. 35

[90] A. AZUMA, S. AZUMA, I. WATANABE, AND T. FURUTA. **Flight mechanics of a dragonfly**. *J. Exp. Biol.*, **116**(1):79–107, 1985. 36

[91] W. J. MAYBURY AND F. O. LEHMANN. **The fluid dynamics of flight control by kinematic phase lag variation between two robotic insect wings**. *J. Exp. Biol.*, **207**(26):4707–4726, 2004. 36

[92] Z. J. WANG AND D. RUSSELL. **Effect of forewing and hindwing interactions on aerodynamic forces and power in hovering dragonfly flight**. *Phys. Rev. Lett.*, **99**(14):148101, 2007. 36

[93] J. R. USHERWOOD AND F. O. LEHMANN. **Phasing of dragonfly wings can improve aerodynamic efficiency by removing swirl**. *J. Roy. Soc. Interface*, **5**(28):1303–1307, 2008. 36

[94] D. RIVAL, D. SCHÖNWEITZ, AND C. TROPEA. **Vortex interaction of tandem pitching and plunging plates: a two-dimensional model of hovering dragonfly-like flight**. *Bioinsp. Biomim.*, **6**(1):016008, 2011. 36

[95] C. K. KANG, H. AONO, C. E. S. CESNIK, AND W. SHYY. **Effects of flexibility on the aerodynamic performance of flapping wings**. *J. Fluid Mech.*, **689**(1):32–74, 2011. 37

[96] G. BIMBARD, D. KOLOMENSKIY, O. BOUTELEUX, J. CASAS, AND R. GODOY-DIANA. **Force balance in the take-off of a pierid butterfly: relative importance and timing of leg impulsion and aerodynamic forces**. *J. Exp. Biol.*, **216**(18):3551–3563, August 2013. 39, 40, 41, 42

[97] S. RAMANANARIVO, B. THIRIA, AND R. GODOY-DIANA. **Elastic swimmer on a free surface**. *Phys. Fluids*, **26**(9):091112, September 2014. 43, 46

[98] S RAMANANARIVO, R GODOY-DIANA, AND B THIRIA. **Propagating waves in bounded elastic media: Transition from standing waves to anguilliform kinematics**. *EPL (Europhysics Letters)*, **105**:1–5, March 2014. 43, 46, 47

[99] V RASPA, S RAMANANARIVO, B THIRIA, AND R GODOY-DIANA. **Vortex-induced drag and the role of aspect ratio in undulatory swimmers**. *Phys. Fluids*, **26**:041701, 2014. 43, 49, 50, 51

[100] R. FERNÁNDEZ-PRATS, V. RASPA, B. THIRIA, F. HUERA-HUARTE, AND R. GODOY-DIANA. **Large-amplitude undulatory swimming near a wall**. *Bioinsp. Biomim.*, **10**:016003, 2015. 43, 57

[101] G. I. TAYLOR. **Analysis of the Swimming of Long and Narrow Animals**. *Proc. Roy. Soc. London. Series A. Mathematical and Physical Sciences*, **214**(1117):158–183, 1952. 44

[102] M. J. LIGHTHILL. **Note on the swimming of slender fish**. *J. Fluid Mech.*, **9**(02):305–317, 1960. 44, 45, 48

[103] J GRAY AND GJ HANCOCK. **The propulsion of sea-urchin spermatozoa**. *J. Exp. Biol.*, **32**(4):802, 1955. 44

[104] C. ELOY, N. KOFMAN, AND L. SCHOUVEILER. **The origin of hysteresis in the flag instability**. *J. Fluid Mech.*, **691**:583–593, January 2012. 44

[105] M. J. LIGHTHILL. **Aquatic animal propulsion of high hydromechanical efficiency**. *J. Fluid Mech.*, **44**(02):265–301, 1970. 44

[106] M. J. LIGHTHILL. **Large amplitude elongated-body theory of fish locomotion**. *Proc. R. Soc. Lond. B Biol. Sci.*, **179**:125–138, 1971. 45

[107] F. CANDELIER, F. BOYER, AND A. LEROYER. **Three-dimensional extension of Lighthill's large-amplitude elongated-body theory of fish locomotion**. *J. Fluid Mech.*, **674**:196–226, 2011. 45

[108] M. J. SHELLEY AND J. ZHANG. **Flapping and Bending Bodies Interacting with Fluid Flows**. *Annu. Rev. Fluid Mech.*, **43**(1):449–465, January 2011. 46

[109] W. W. SCHULTZ AND P. W. WEBB. **Power requirements of swimming: do new methods resolve old questions?** *Integr. Comp. Biol.*, **42**(5):1018–1025, 2002. 49

[110] R. BALE, M. HAO, A. P. S. BHALLA, AND N. A. PATANKAR. **Energy efficiency and allometry of movement of swimming and flying animals**. *Proc. National Ac. Sci. (USA)*, **111**(21):7517–7521, May 2014.

[111] U. EHRENSTEIN, M. MARQUILLIE, AND C. ELOY. **Skin friction on a flapping plate in uniform flow**. *Phil. Trans. Roy. Soc. A*, **372**(2020):20130345–20130345, June 2014. 49

[112] J. BRACKENBURY. *Insects in Flight*. Blandford, London, 1995. 54

[113] A. BELKHIRI, M. POREZ, AND F. BOYER. **A hybrid dynamic model of an insect-like MAV with soft wings**. In *Robotics and Biomimetics (ROBIO), 2012 IEEE International Conference on*, pages 108–115, Dec 2012. 53

[114] K. Y. MA, P. CHIRARATTANANON, S. B. FULLER, AND R. J. WOOD. **Controlled Flight of a Biologically Inspired, Insect-Scale Robot**. *Science*, **340**(6132):603–607, 2013. 54

[115] W. R. CHAN, P. BERMEL, R. C. N. PILAWA-PODGURSKI, C. H. MARTON, K. F. JENSEN, J. J. SENKEVICH, J. D. JOANNOPOULOS, M. SOLJAČIĆ, AND I. CELANOVIC. **Toward high-energy-density, high-efficiency, and moderate-temperature chip-scale thermophotovoltaics**. *Proc. National Ac. Sci. (USA)*, **110**(14):5309–5314, 2013. 54

[116] M. J. MCHENRY AND G. V. LAUDER. **The mechanical scaling of coasting in zebrafish (Danio rerio)**. *J. Exp. Biol.*, **208**(12):2289–2301, June 2005. 54, 55

[117] J. W. M. BUSH, D. L. HU, AND M. PRAKASH. **The integument of water-walking arthropods: form and function**. In J. CASAS AND S. J. SIMPSON, editors, *Insect Mechanics and Control*, **34** of *Advances in Insect Physiology*, pages 117–192. Elsevier, 2008. 55

[118] J. W. TAVACOLI, P. BAUËR, M. FERMIGIER, D. BARTOLO, J. HEUVINGH, AND O. DU ROURE. **The fabrication and directed self-assembly of micron-sized superparamagnetic non-spherical particles** . *Soft Matter*, **9**(38):9103–9110, 2013. 55

[119] B. J. NELSON, I. K. KALIAKATSOS, AND J. J. ABBOTT. **Microrobots for minimally invasive medicine**. *Annu. Rev. Biomed. Eng.*, **12**:55–85, 2010. 55

[120] F.P. GOSSELIN, D. ZHOU, V. LALANDE, M. VONTHRON, AND S. MARTEL. **Miniature ferromagnetic robot fish actuated by a clinical magnetic resonance scanner**. In *Intelligent Robots and Systems (IROS), 2011 IEEE/RSJ International Conference on*, pages 901–906, Sept 2011. 55

[121] S. MARTEL, J. B. MATHIEU, O. FELFOUL, H. MACICIOR, G. BEAUDOIN, G. SOULEZ, AND L. H. YAHIA. **Adapting MRI systems to propel and guide microdevices in the human blood circulatory system**. In *Engineering in Medicine and Biology Society, 2004. IEMBS'04. 26th Annual International Conference of the IEEE*, **1**, pages 1044–1047. IEEE, 2004. 55

[122] M. C. MARCHETTI, J. F. JOANNY, S. RAMASWAMY, T. B. LIVERPOOL, J. PROST, M. RAO, AND R. A. SIMHA. **Hydrodynamics of soft active matter**. *Rev. Mod. Phys.*, **85**(3):1143, 2013. 56

[123] G. MIÑO, T. E. MALLOUK, T. DARNIGE, M. HOYOS, J. DAUCHET, J. DUNSTAN, R. SOTO, Y. WANG, A. ROUSSELET, AND E. CLEMENT. **Enhanced Diffusion due to Active Swimmers at a Solid Surface**. *Phys. Rev. Lett.*, **106**(4):048102, January 2011. 56

[124] R. M. HARSHEY AND T. MATSUYAMA. **Dimorphic transition in Escherichia coli and Salmonella typhimurium: surface-induced differentiation into hyperflagellate swarmer cells**. *Proc. National Ac. Sci. (USA)*, **91**(18):8631–8635, 1994. 56

[125] D. CROWDY, S. LEE, O. SAMSON, E. LAUGA, AND A. E. HOSOI. **A two-dimensional model of low-Reynolds number swimming beneath a free surface**. *J. Fluid Mech.*, **681**:24–47, August 2011. 56

[126] G. J. LI AND A. M. ARDEKANI. **Hydrodynamic interaction of microswimmers near a wall**. *Phys. Rev. E*, **90**(1):013010, July 2014. 56

[127] T. S. YU, E. LAUGA, AND A. E. HOSOI. **Experimental investigations of elastic tail propulsion at low Reynolds number**. *Phys. Fluids*, **18**(9):091701, 2006. 56

[128] J. ESPINOSA-GARCIA, E. LAUGA, AND R. ZENIT. **Fluid elasticity increases the locomotion of flexible swimmers**. *Phys. Fluids*, **25**(3):031701, 2013.

[129] B. J. WILLIAMS, S. V. ANAND, J. RAJAGOPALAN, AND M. T. A. SAIF. **A self-propelled biohybrid swimmer at low Reynolds number**. *Nat. Comm.*, **5**:1–8, January 2014.

[130] I. S. M. KHALIL, H. C. DIJKSLAG, L. ABELMANN, AND S. MISRA. **MagnetoSperm: A microrobot that navigates using weak magnetic fields**. *Appl. Phys. Lett.*, **104**(22):223701, June 2014. 56

[131] S. J. CASSELMAN, A. I. SCHULTE-HOSTEDDE, AND R. MONTGOMERIE. **Sperm quality influences male fertilization success in walleye (sander vitreus)**. *Can. J. Fish. Aquat. Sci.*, **63**:2119–2125, 2006. 56

[132] R. ZENIT AND R. GODOY-DIANA. **Synthetic C-start maneuver in fish-like swimming**. 2014. In preparation. 58

[133] A. HERREL, S. E. VINCENT, M. E. ALFARO, S. VAN WASSENBERGH, B. VANHOOYDONCK, AND D. J. IRSCHICK. **Morphological convergence as a consequence of extreme functional demands: examples from the feeding system of natricine snakes**. *J. Evol. Biol.*, **21**(5):1438–1448, September 2008. 59

[134] J. J. ALLEN AND A. J. SMITS. **Energy harvesting eel**. *J. Fluids Struct.*, **15**(3):629–640, 2001. 59

[135] K. SINGH, S. MICHELIN, AND E. DE LANGRE. **The effect of non-uniform damping on flutter in axial flow and energy-harvesting strategies**. *Proc. Roy. Soc. A*, **468**(2147):3620–3635, September 2012.

[136] S. MICHELIN AND O. DOARÉ. **Energy harvesting efficiency of piezoelectric flags in axial flows**. *J. Fluid Mech.*, **714**:489–504, January 2013. 59

[137] H. M. NEPF. **Flow and Transport in Regions with Aquatic Vegetation**. *Annu. Rev. Fluid Mech.*, **44**(1):123–142, January 2012. 59

Short bio

Ramiro Godoy-Diana (born in 1972 in Buenos Aires, Argentina), is a CNRS research scientist at the Physique et Mécanique des Milieux Hétérogènes laboratory (PMMH) at ESPCI in Paris, France. Physical engineer from the Tec de Monterrey (México, 1994), he holds a Master in Physics from the UNAM (México, 1999) and a PhD in fluid dynamics from École Polytechnique (France, 2004). His experimental fluid dynamics work has included research on ocean wave energy, geophysical fluid dynamics, wake instabilities, fluid-structure interaction and bio-inspired propulsion. The latter being his current major field of work.

Contact:


```
PMMH-ESPCI, 10, rue Vauquelin, 75231 Paris Cedex 05 FRANCE
e-mail ramiro@pmmh.espci.fr
web http://blog.espci.fr/ramiro/
tel +33140794716 fax +33140794523
```


Career history:

since 10/2006	CNRS researcher (CR1 since 10/2010). PMMH
2005-2006	Postdoc CNRS. PMMH
2004-2005	Postdoc and Temporary teaching/research fellow (ATER). Oceanography Laboratory (LOCEAN). UPMC.
2000-2004	PhD research. LadHyX, École Polytechnique.
1997-1999	Junior researcher. Wave Energy team. ICMyL-UNAM.

Recent grants:

- EADS foundation: "Fluids and elasticity in biomimetic propulsion" 2012-2014
- ANR “programme blanc” project ENTOMOPTER 2008-2012

PhD students and postdocs:

Intesaaf Ashraf (PhD student 2014-2017, co-advised with B. Thiria)
Marion Segall (PhD student 2014-2017, co-advised with A. Herrel)
Miguel Piñeirua (Postdoc 2014-2015, co-advised with B. Thiria)
Verónica Raspa (Postdoc 2010-2013, co-advised with B. Thiria)
Sophie Ramananarivo (PhD student 2010-2013, co-advised with B. Thiria)
Catherine Marais (PhD student 2007-2010, co-advised with J. E. Wesfreid)

Appendix: Selected publications

The following articles are available for download on my website at ESPCI:

`http://blog.espci.fr/ramiro/`

TRANSITIONS IN THE WAKE OF A FLAPPING FOIL
GODOY-DIANA, AIDER, WESFREID *Phys. Rev. E* **77**, 016308 (2008).

A MODEL FOR THE SYMMETRY BREAKING OF THE REVERSE BÉNARD-VON KÁRMÁN VORTEX STREET PRODUCED BY A FLAPPING FOIL.
GODOY-DIANA, MARAIS, AIDER, WESFREID *J. Fluid Mech.* **622**, 23-32 (2009).

STABILIZING EFFECT OF FLEXIBILITY IN THE WAKE OF A FLAPPING FOIL.
MARAIS, THIRIA, WESFREID, GODOY-DIANA *J. Fluid Mech.* **710**, 659-669 (2012).

TOPOLOGY-INDUCED EFFECT IN BIOMIMETIC PROPULSIVE WAKES.
RASPA, GODOY-DIANA, THIRIA *J. Fluid Mech.* **729**, 377-387 (2013).

HOW WING COMPLIANCE DRIVES THE EFFICIENCY OF SELF-PROPELLED FLAPPING FLYERS.
THIRIA, GODOY-DIANA *Phys. Rev. E* **82**, 015303R (2010).

RATHER THAN RESONANCE, FLAPPING WING FLYERS MAY PLAY ON AERODYNAMICS TO IMPROVE PERFORMANCE.
RAMANANARIVO, GODOY-DIANA, THIRIA *Proc. Natl. Acad. Sci. (USA)* **108** (15), 5964-5969 (2011).

FOREWING-HINDWING PHASE-LAG EFFECT IN THE PROPULSIVE PERFORMANCE OF A FOUR-WINGED FLAPPING FLYER.
GODOY-DIANA, JAIN, CENTENO, WEINREB, THIRIA . IN *Selected Topics of Computational and Experimental Fluid Mechanics, Environmental Science and Engineering.* (KLAPP ET AL., EDITORS) SPRINGER (2015, IN PRESS).

FORCE BALANCE IN THE TAKE-OFF OF A PIERID BUTTERFLY: RELATIVE IMPORTANCE AND TIMING OF LEG IMPULSION AND AERODYNAMIC FORCES.
BIMBARD, KOLOMENSKIY, BOUTELEUX, CASAS, GODOY-DIANA *J. Exp. Biol.* **216**, 3551-3563 (2013).

PASSIVE ELASTIC MECHANISM TO MIMIC FISH-MUSCLES ACTION IN ANGUILLIFORM SWIMMING
RAMANANARIVO, GODOY-DIANA, THIRIA *J. Roy. Soc. Interface* **10**, 20130667 (2013).

PROPAGATING WAVES IN BOUNDED ELASTIC MEDIA: AN APPLICATION TO THE EFFICIENCY OF BIO-INSPIRED SWIMMERS
RAMANANARIVO, GODOY-DIANA, THIRIA. *EPL*, **105**, 54003 (2014).

VORTEX-INDUCED DRAG AND THE ROLE OF ASPECT RATIO IN UNDULATORY SWIMMERS
RASPA, RAMANANARIVO, THIRIA, GODOY-DIANA. *Phys. Fluids*, **26**, 041701 (2014).

ELASTIC SWIMMER ON A FREE SURFACE
RAMANANARIVO, THIRIA, GODOY-DIANA. *Phys. Fluids*, **26**, 091112, (2014, GALLERY OF FLUID MOTION).

LARGE-AMPLITUDE UNDULATORY SWIMMING NEAR A WALL
FERNÁNDEZ-PRATS, RASPA, THIRIA, HUERA-HUARTE, GODOY-DIANA. *Bioinsp. Biomim.*, **10**, 016003 (2015).